CHAPTER 1

INTRODUCTION

1.1 General

The centrifugal pump casing guides the liquid from the suction connection to the centre, or eye, of the impeller. The vanes of the rotating impeller impart a radial and rotary motion to the liquid, forcing it to the outer periphery of the pump casing wherein it's miles accrued inside the outer a part of the pump casing referred to as the volute. The volute is a vicinity that expands in cross-sectional place because it wraps around the pump casing. The motive of the volute is to collect the liquid discharged from the outer edge of the impeller at excessive velocity and progressively reason a reduction in fluid speed by growing the waft area. This converts the speed head to static stress. The fluid is then discharged from the centrifugal pump thru the discharge connection. Cavitation (from hollow space) is defined as the speedy formation and fall apart of vapour bubbles or pockets in a liquid, because of dynamic motion, and resulting in the formation of cavities on the surfaces of stable barriers. these stable barriers can exist in any number of structures along with hydrofoils, pipes, and fittings however, in our enterprise, the number one victims are impellers and propellers.

The purpose of this thesis is to assist to advantage an intuitive information of the cavitation technique and its reasons. i can go away its prevention to the various articles that exist already. since boiling is the precursor to cavitation, we can begin by taking a have a look at a number of the properties of water and their position inside the cavitation

procedure. we are able to then put NPSH into attitude and overview a number of the dynamics of centrifugal pump operation that also directly affect the method. we will conclude with a discussion of the exclusive kinds of centrifugal pump cavitation and the conditions which could purpose them to arise.

Physics Of Cavitation In Liquid Flows

Cavitation is the process of formation of vapor bubbles in a liquid go with the flow caused by an initial discount of strain under vapor pressure, and next disintegrate of the bubbles due to a strain growth. here stress approach absolute strain referenced against a really perfect vacuum (zero Pa).

When vapor cavities have started to form cavitation bubbles, they may be transported by using the flowing liquid. whilst flowing thru low pressure zones they may extend because of the stress variations among the vapor within the bubbles and the encompassing liquid. In zones with higher strain the bubbles will settlement. The price of this expansion or contraction might be confined via the forces of surface anxiety and viscous forces.

When the bubbles agreement closer to an infinitely small radius, they'll implode in a instead violent disintegrate caused by excessive strain on the middle of the bubble. The crumble is accompanied by way of a localized strain pulse which can deliver upward push to small but powerful micro jets. those two consequences can damage the encompassing surfaces.

The cavitation process occur in two phases

First Phase – Bubble formation happens at a point in which the pumping liquid strain is less than the vapor pressure

Second Phase – The bubble fall apart or implosion happens at a point wherein the pressure will boom above the vapor pressure.

1.2 Aim And Objectives

The main objective of this work is to present cavitation modeling in centrifugal pump impeller via ANSYS 18.2 CFX, so that it can reduce cost, exact place at which maximum cavitation occurs, intensity of cavitation at different location, reduce time as well as men's power. Also how the operating conditions and input parameters affect the impeller geometry.

The aim of this thesis is to accurately predict the cavitation of the centrifugal pump with the help of Computational Fluid Dynamics (CFD).

1.3 Numerical Analysis

Computational Fluid Dynamics (CFD) is a powerful tool used to model the real life behaviour of fluids. It allows the optimization of design parameters without the need for the costly testing of multiple prototypes. What is more, it is also a powerful graphical tool for visualizing flow patterns that can give insight into flow physics that otherwise would be very difficult and costly to discover experimentally, if possible at all. Governing equations exist to model fluid behaviour, but it is not always possible to apply them to many of the complex flow patterns we see in the real world directly as there would be too many unknown variables. However, CFD involves creating a computational mesh to divide up real world continuous fluids into more manageable discrete sections. The governing equations for fluid flow can then be applied to each section individually, but as the properties of each section are inevitably linked to its neighbouring sections, all the sections can be solved simultaneously until a full solution for the entire flow field can be found. This method obviously requires a huge amount of computational power, nevertheless with the advancement of modern computing, solutions that would take months to compute by hand can now be found in seconds using nothing more than an ordinary desktop or laptop computer.

As with everything, CFD is not without its limitations. Its accuracy or validity are dependent on a multitude of different factors: the quality and appropriateness of the mesh,

the degree to which the chosen equations match the type of flow to be modelled, the interpretation of the results, the accuracy of the boundary conditions entered by the user or the level of convergence of the solution, to name but a few. Often it comes down to the skill of the user, as each flow problem will be slightly different and as a result, will require a slightly different modelling approach. However, experimental data can provide a valuable reference point with which to check the validity of CFD models.

1.4 Research Methodology

Cavitation Effects-Now we will see the effect of cavitation in pump during the first and second phase**.**

Cavitation Effect On Bubble Formation Phase

On this phase, the pumping liquid drift is decreased as the liquid is displaced by way of vapor. due to this, a mechanical imbalance takes place as the impeller passages are fill with lighter vapors. This consequences in vibration and shaft deflection, ultimately resulting in bearing disasters, packing or seal leakage, and shaft breakage. within the case of multi-degree pumps, this can reason lack of thrust stability and thrust bearing failures.

Cavitation Effect On Bubble Collapse Phase

1. Mechanical damage occurs as the imploding bubbles remove segments of impeller material.
2. Noise and vibration result from the implosion. The noise that sounds like gravel is the user's first warning of cavitation

Reason for Cavitation

NPSH (R) exceeds NPSH (A)

Due to low pressure, the water vaporizes (boils) and higher pressure implodes into the vapor bubbles as they pass through the pump causing reduced performance and potentially major damage.

Suction Or Discharge Recirculation

The pump is designed for a certain flow range if there is not enough or too much flow going through the pump. The resulting is turbulence and vortexes can reduce performance and damage the pump.

Prevent Centrifugal Pump Cavitation

While designing a pumping system or selecting a pump, one must thoroughly evaluate Net Positive Suction Head (NPSH) margin to prevent cavitation.

Net Positive Suction Head (NPSH) margin = NPSHA – NPSHR

Proper analysis of both the net positive suction heads available in the system (NPSHA) and the net positive suction head required by the pump (NPSHR) will reduce the formation of cavitation

NPSH Available*:* It is a degree of the strain drop as the liquid travels from the pump suction flange along the inlet to the pump impeller. This loss is due primarily to friction and turbulence.

Turbulence loss is extraordinarily high on the low drift of the pump after which decreases with drift closer to the best performance point of the pump. Friction loss commonly will increase with the growth in pump waft fee. As a end result, the internal pump losses can be high at low glide, dropping at generally 20–30% of the pleasant efficiency drift, then increasing with the glide. The NPSHr of the pump is reap from the real pump curve. The pump manufacturer determines the actual NPSHR for each pump over its entire operating variety with the aid of a sequence of testsThe element check manner is describe in the Hydraulic Institute check standard 1988, Centrifugal Pumps 1.6.The industry has agreed on a 3% head reduction at consistent drift as the usual cost to set up NPSHR. (Refer below parent).

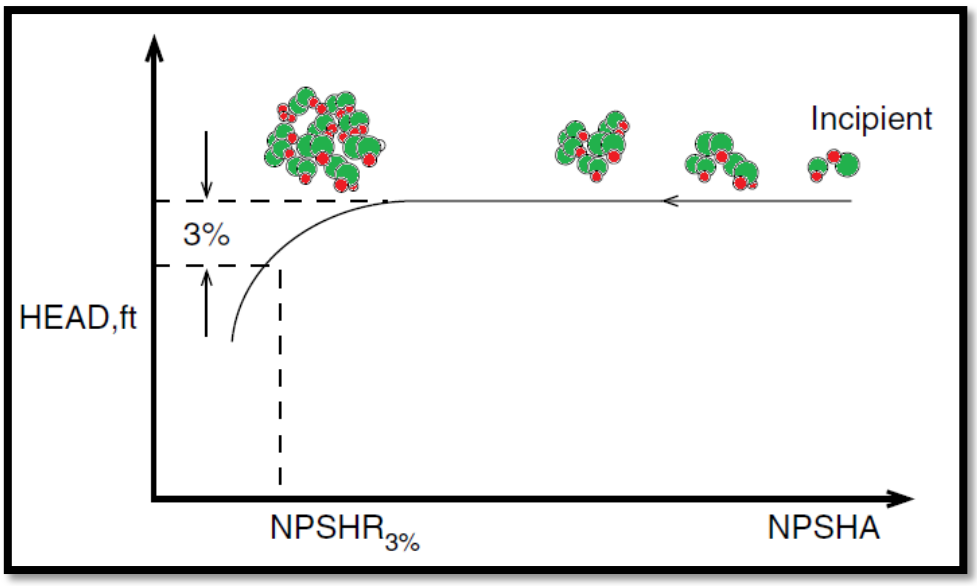

FIGURE 1.1 HEAD vs $NPSH_A$

The NPSH margin required will vary with pump design and other factors, and the exact margin cannot be precisely predicted. For most applications, the NPSHA will exceed the NPSHR. Normally the NPSH margin will be of 1m is consider for pump selection to avoid cavitation.

1.5 Computational Fluid Dynamics (CFD)-

Qiu, et al., (2010) defined that the design manner typically utilized in turbomachinery has numerous exclusive tiers, with every level having a separate function. the first step of the integrated design system is the evaluation of the machine as an entire which turned into accomplished. This entails figuring out the type of machinery wanted as well as the primary working conditions of the level/gadget. the following stage is the one dimensional (1D) meanline evaluation in which the design necessities are exact. The concept is to decide the flow route and geometry in addition to the potential performance of the device. The 1D analysis has a quick turnaround time but the reliance on empirical fashions way that careful validation is needed to make sure the integrity of the result. The

meanline application is the starting point of a brand new design. The meanline system plays two most important tasks. the first is the production of a new design with unique working situations. the second one mission is to are expecting the overall performance of an existing design with the secondary tasks together with choke, stall and cavitation predictions.

As soon as the 1D outcomes have been evolved, a three-D geometry for the drift route and blading can be generated. This geometry may be refined through the usage of second and 3-D solvers via interactively changing sure geometric information until a very last optimized design has been reached. but, the addition of an additional size (3-D) approach the solver run time can be expanded. the very best level of analysis is complete 3 dimensional CFD. but, that is the most computationally highly-priced solver because it permits the whole drift field to be resolved with minimal compromise. The design can be in addition subtle with the aid of the use of CFD to obtain the preferred go with the flow discipline. because the layout space is narrowed via the incorporated layout technique, the optimization process becomes greater efficient making CFD the pleasant tool for designated optimization. once the numerical answer for the complete drift area has been computed the usage of CFD the results may be as compared to the original layout. If the three-D numerical solution does no longer meet positive output standards, the designer ought to move back to the 1D meanline software to likely refine the layout and regulate the geometry.

CFD is a totally powerful engineering tool that allows a extensive style of float situations to be simulated and understood whilst also having the additional benefits that it is able to both reduce the quantity of checking out required or it can be used to validate certain checks.

CFD calculations are based totally at the three crucial equations of fluid dynamics, specifically: the conservation of mass, momentum and strength. those equations form the Navier Stokes equations, which can be a set of partial differential equations (PDEs) that, in most people of cases, do now not have an analytical solution. but, PDEs may be approximated by using a hard and fast of algebraic equations via using a discretisation method. there are various discretisation techniques, the maximum not unusual being the finite element approach, the finite difference technique and the finite volume approach. In

essence the approximated algebraic equations are applied to small sub-volumes inside the glide; a procedure that's repeated numerous instances that allows you to cover the complete volume of the glide.

Commonly a CFD simulation follows a particular system that includes several levels which can be defined below (de Souza, 2013). those ranges are trendy degrees for all CFD software and vary barely for each man or woman software program package.

The primary degree is the approximation of the geometry. The geometry is advanced in a 3 dimensional modelling application and desires to be as accurate as feasible if it's far to copy the overall performance of the actual gadget. The geometry is then imported into the applicable CFD software program package deal.

The next degree includes the choice of the physics models which constitute the float characteristics. The mathematical models and parameters for the go with the flow phenomena are decided on and the boundary situations are described for the area.

The fourth level offers with the prescription of initial situations. Discretisation effects in a massive wide variety of algebraic equations which might be solved iteratively whereby a guess is made for the primary set of variables. errors values (residuals) are computed from the discretised equations and the calculations are repeated severa instances till the residuals values have decreased sufficiently and the solution is judged to have converged. The preliminary situations specify the fee of the fluid variables at some stage in the flow domain at the start line of a simulation.the following degree is determining whether or no longer the solution has converged as so been run. when the sum of the residual values has come to be sufficiently small, the answer is taken into consideration converged. some other test is that the additional iterations produce negligible versions in different outputs being measured which includes drag coefficient or stress.

The final level of jogging a CFD simulation is solution verification and validation. preferably, every solution need to be as compared to theoretical calculations or experimental records. inside the current studies a evaluation with experimental information isn't viable because the experimental rig stays incomplete, consequently, the assessment this is offered relies totally at the effects obtained from the 1D software (PUMPAL) as used

by Smyth (2013). This development changed into beyond the manipulate of the writer. at the outset of this venture the goal become to evaluate the CFD evaluation with the experimental outcomes and feature the validation required to properly investigate the meanline layout of the total scale impeller.

Lamentably, the complex alterations required for the volute casing have not but been finished. The check rig additionally requires similarly changes to the inlet piping in an effort to visually check the cavitation.

1.6 Indicators Of Pump Cavitation

Noise And Vibration

The onset of cavitation is regularly first detected by emitted noise instead of by using visual remark of bubbles, cloth damage or reduced performance. The damn sound that accompanies cavitation is one of the maximum demanding traits of this phenomenon, with frequencies from 10 kHz to a hundred kHz. The direct noise from cavitation within the pumped liquid is seldom the problem, however it is able to be transmitted thru solid structures, each within the pump and inside the surrounding pipe system. For large dry-installed pumps the energy in cavitation-triggered vibrations can every now and then reason severe noise in addition to harm to the pump and the piping device.

FIG. 1.2 PUMP IMPELLER

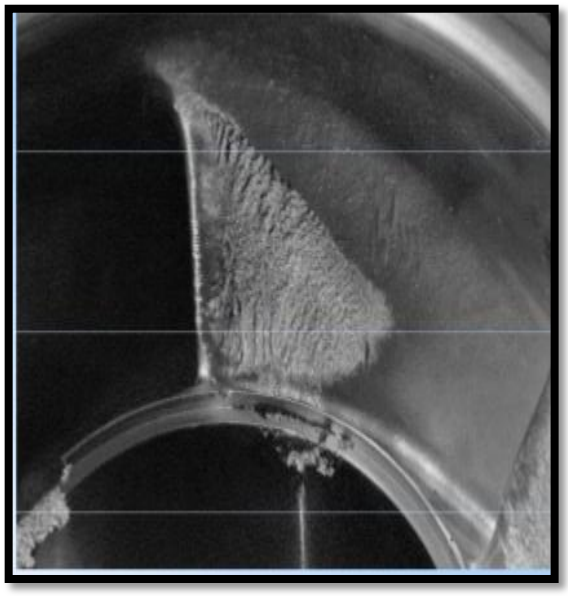

FIG 1.3 FRANCIS TURBINE

Surface Damage

Possibly the most apparent impact of cavitation on pumps is the fabric damage that cavitation bubbles can reason when they collapse in the vicinity of a stable surface. in the end, this ends in fatigue failure and the following detachment or flaking off of portions of cloth. The severity of the damage is dependent on the houses of each impeller material and the pumped liquid.

Corrosion will regularly increase the rate of deterioration. for the reason that oxides are much less resilient to surface fatigue than the natural metal, cavitation constantly chips off portions of the oxide layer which protects the metal. This non-stop publicity of a fresh metal surface accelerates the corrosion method. therefore, the cavitation and the corrosion progresses are compounded.

Cavitation behavior is typically expressed in terms of cavitation parameters.

Cavitation number:

$$\sigma = \frac{\rho_1 - \rho_v}{\frac{1}{2}\rho U^2}$$

1.7 Impact On Performance

Cavitation reduces the pinnacle and the energy of the pump as the vapor bubbles will reduce the energetic impeller passage. A small quantity of cavitation will in many instances exchange the pump head and strength in an unpredictable way with the aid of changing the pressure distribution across the impeller blades. In uncommon instances this effect may even improve the pump performance; a misleading phenomenon for pump operatives.

CHAPTER 2

LITERATURE REVIEW

A literature review was conducted to further understand the CFD process, the different techniques and models as well as the basics of cavitation; a flow phenomena which limits the negative pressures that can be tolerated in a liquid flow. The following chapter deals with the various categories of CFD relevant to this study. Naturally this involves the different types of mesh and turbulence models. The chapter also deals with several key papers which are similar to the work at hand. Cavitation is also discussed as well as the modelling parameters that predict its formation.

2.0 COMPUTAIONAL FLUID DYNAMICS –

2.1 Mesh Models

As already stated, the governing equations are discretised before they are solved. The most common technique for discretisation in fluid simulations is the Finite Volume Method (FVM). The Finite Difference Method was more popular in the past but has a lack of flexibility when compared to the FVM. The Finite Element Method is also popular but more so in multiphysics simulations which are simulations where several physical phenomena are present and coupled systems of partial differential equations are required (De Beristain, 2012).

In the Finite Volume Method the domain is divided into a finite number of control volumes which correspond to the cells of a computational grid. Discrete versions of the integral form of the governing equations are then applied to each control volume in the domain. Star CCM+ uses the FVM to discretise these governing equations and obtain a set of linear algebraic equations which are solvable. This software formed the basis of the author's work.

The mesh of the computational domain is the discretised representation of the domain which is used by the solvers to provide a numerical solution. Star CCM+ has various mesh tools (surface and volume) and models available to accurately represent different geometries.

Naturally, an important aspect of any fluid simulation that encounters turbulence is the boundary layer. To capture the boundary layer flow accurately the Prism Layer Mesher is used. This mesh model projects the core mesh back to the wall boundaries to create orthogonal prismatic cells next to the wall an example of which can be seen in figure 2.1.

.

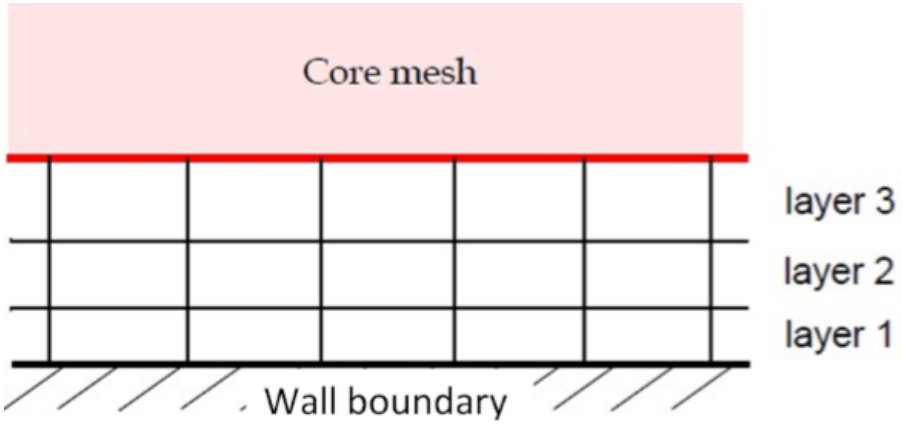

FIGURE 2.1 AN EXAMPLE OF 3 PRISM LAYER

The distribution of the prism layers is linked to the wall y+ value of the model. The y+ value is an indication of how accurately the mesh will capture the boundary layer. A low y+ (<1) means that the first cell centroid is within the viscous sublayer of the flow which will result in an accurate depiction of the boundary layer. A high y+ (30< y+ <100) means that the near wall cell centroid is in the loglaw region of the boundary layer. The ideal y+

value for an impeller of this nature is debatable. Montomoli, et al., (2010) aimed for a y+ value of 1 in their study of the tip gap and fillet radius effects in turbomachinery while Lucius & Brenner, (2010) use only a Y+ value of 3.1. Westra, et al., (2010) also deemed a Y+ value of 3 to be sufficient while (Balasubramanian, et al., 2011) were content with a Y+ of 5.

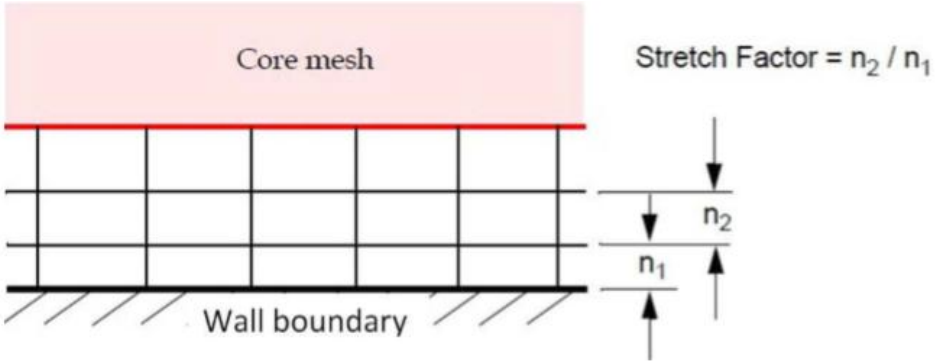

FIGURE 2.2 STRETCH FACTOR

As stated, the value of the wall Y+ can be set by defining the thickness of the prism layer closest to the wall. Equation 2.1 shows how the Y+ value can be calculated. In this equation, is the distance from the wall to the first cell centroid. By selecting a Y+ value, the thickness of the first cell can be calculated. The thickness can then be prescribed in Star CCM+ after altering the method used to define the prism layers. The Y+ value is also dependent on the reference velocity,(which is a function of the wall shear stress, , and density) as well as the kinematic viscosity of the fluid.

$$y^+ = \frac{U^* Y}{V}$$

$$U^* = \sqrt{\frac{\tau_W}{\rho}}$$

2.2 Turbulence Modeling

One of the main obstacles in modeling Turbomachinery flows is the accurate modeling of the turbulence that is present in the flow field. Several methods described below are used to model the turbulence in fluid flow. Due to the popularity and convenience of the Reynolds Averaged Navier Stokes (RANS) techniques, the author has provided a more in-depth look at these models. Literature suggests (Ferziger & Peric, 2002) the best way to approach turbulence modelling is to use a RANS technique as a starting point and if the results are inadequate, move on to a more in depth technique such as Large Eddy Simulations (LES) or Direct Numerical Simulations (DNS) (if the computing power is available). While DNS may be the most accurate way to simulate turbulence, the computational expense generally outweighs the accuracy. Montomoli, et al., (2010) used the KOmega model to model the flow behaviour at the rotor tip to see how small geometric differences affect the flow behaviour. Ranade & Krishnan (2002) argued that the K-Epsilon model was inadequate in modelling the flow around an impeller. Despite this, Ranade & Krishnan (2002) stated that in most cases the mesh quality affected the accuracy of results more than the turbulence model being used and that if the turbulence model yielded reasonable results, it was not necessary to use a more complex model. Jafarzadeh, et al., (2010) performed a comparison between K-Epsilon, ReNormalisation Group (RNG) K-Epsilon and Reynolds Stress Model (RSM), finding that the standard K-Epsilon model provided the least accurate results when compared to a particular experimental data set. However Barrio, et al., (2010) also used the standard K-Epsilon model but found the results accurate to within 4% of the experimental data. Bacharoudis, et al., (2008) used the K-Epsilon successfully, claiming that the numerical predictions predicted the total performance as well as the global characteristics of the laboratory pump reasonably well compared to experimental data. Shojaeefard, et al., (2012) used the Shear Stress Transport (SST) K-Omega model due to its high precision when modelling near-wall flow when looking at the performance of a centrifugal pump when certain geometric characteristics of the pump were altered. The numerical predictions of Shojaeefard, et al., (2012) were within 4% of the experimental results when using the SST K-Omega turbulence model. This information generally illustrates that different turbulence models are sensitive to the application at hand and are not universally better. The current work will use the SST-

Menter KOmega model, for reasons discussed in the information below. A brief description of the different turbulence models is presented below, with a more in depth look at the two most popular turbulence models, namely the K-Omega and K-Epsilon models.

2.3 Direct Numerical Simulation

The most accurate approach to turbulence simulation is Direct Numerical Simulation whereby the Navier-Stokes equations are solved without averaging or approximation (Ferziger & Peric, 2002). In Direct Numerical Simulation the Navier-Stokes equations are solved to determine the velocity field for one realization of the flow. DNS is especially computationally expensive because all length scales and timescales have to be resolved, in other words all the motions in the flow are resolved. The approach is also restricted to flows with a low Reynolds number as the computational cost increases at a rate proportional to the cube of the Reynolds number (Re3) (Pope, 2000). Due to the comprehensive nature of the results obtained using DNS it is too expensive to be used as a design tool and should rather be used as a research tool to create numerical flow visualization (Ferziger & Peric, 2002). Due to the high computational cost of DNS, it is not available in many commercial software packages and was not considered a viable option for this study. Some examples of where DNS has been used are:

1. Understanding the mechanisms of turbulence production, energy transfer and dissipation in turbulent flows
2. Simulation of the production of aerodynamic noise
3. Understanding the effects of compressibility on turbulence
4. Understanding the interaction between combustion and turbulence
5. Controlling and reducing drag on a solid surface

2.4 Large Eddy Simulation

In LES, equations are solved for a ‘filtered’ flow field, where the larger turbulent motions are the most important (Pope, 2000). The large scale motions are more energetic than the smaller ones and are effective transporters of the conserved properties, due to their

size and strength. The small scale motions are weaker and provide poor transport of the conserved properties. LES solves for the large scales of the turbulence and models the small scale motions. LES is three dimensional, time dependent and computationally expensive but not when compared to DNS. LES is the preferred method for flows through complex geometries and flows with a high Reynolds number (Ferziger & Peric, 2002)

2.5 Detached Eddy Simulation

Detached Eddy Simulation (DES) is a hybrid modeling approach that applies RANS techniques in some areas of the flow and LES methods in others areas. A DES model uses a base RANS model to solve the shear layers and then uses LES in the unsteady separated region of the flow (CD-ADAPCO, 2013). Majority of DES computations use Spalart-Allmaras as the base model. DES appears to use RANS as the near wall treatment and then LES away from the wall (Viswanathan, 2006).

While the DES approach seems promising for certain types of simulations, it must be noted that DES is not always the solution to turbulence modeling. The creation of a suitable grid is vital when using DES (CD-Adapco, 2013).

The recommended base RANS model is the Spalart-Allmaras detached eddy model. However, the SST (Menter) K-Omega model is also a viable option (CD-Adapco, 2013).

2.6 Reynolds Averaged Navier-Stokes

The oldest approach to turbulence modelling is Reynolds Averaged Navier-Stokes (RANS). In the RANS approach to turbulence, the Navier-Stokes equations for the instantaneous velocity and pressure fields are broken down into a mean and fluctuating component. Then, in the RANS approaches, all of the unsteadiness and fluctuations are averaged out. The RANS approach involves the solution of the Reynolds equations to determine the mean velocity field (Ferziger & Peric, 2002). The Navier Stokes equations

consist of the equations for conservation of mass and momentum, which can be seen in equation 2.3 and 2.4 respectively (Wilcox, 1993)

$$\frac{du_i}{dx_i} = 0 \qquad \ldots.(2.3)$$

$$\rho \frac{du_i}{dt} + \rho u_j \frac{du_i}{dx_j} = -\frac{dP}{dx_i} + \frac{dt_{ji}}{dx_j} \qquad \ldots.(2.4)$$

The vectors and represent velocity and position while t is time, p is pressure, is density and is the viscous stress tensor which is defined by Wilcox as

$$t_{ij} = 2\mu s_{ij} \qquad \ldots.(2.5)$$

Where is the molecular viscosity and is the strain rate tensor,

$$\rho \frac{du_i}{dt} + \rho \frac{d}{dx_j}(u_j\, u_i) = -\frac{dP}{dx_i} + \frac{d(2\mu s_{ji})}{dx_j} \qquad \ldots.(2.6)$$

Combining the above equations yields the Navier Stokes equation in conservation form. Time averaging the conservation of mass and the above Navier Stokes equation results in the Reynolds Averaged equations of motion in conservation form as defined by Wilcox (1993),

$$\frac{dU_i}{dx_i} = 0 \qquad \ldots.(2.7)$$

$$\rho \frac{dU_i}{dt} + \rho U_j \frac{dU_i}{dx_j} = -\frac{dP}{dx_i} + \frac{d}{dx_j}\left(2\mu s_{ji} - \overline{\rho u_j' u_i'}\right) \qquad \ldots.(2.8)$$

Aside from the replacement of the instantaneous variables by mean values, the time-averaged equations are identical to the instantaneous equations with the exception of what is termed the Reynolds Stress Tensor denoted (τ_{ij}) (Wilcox, 1993):

$$\tau_{ij} = -\rho\overline{u_i' u_j'} \quad \ldots.(2.9)$$

Due to the presence of the extra term above, the conservation equations contain more variables than there are equations. So for three dimensional flows there are four mean-flow properties that are unknown (three velocity components and pressure) as well as six Reynolds stress components. This yields ten unknowns and only four equations (the continuity equation and three components of the Navier Stokes equation) (Davidson, 2011) and therefore the system is not closed.

Eddy viscosity models are based on a turbulent viscosity which is computed using an algebraic model. The most common approximation which forms the basis of all eddy viscosity models is the Boussinesq approximation (Davidson, 2011). This assumption relates the Reynolds stress tensor to the velocity gradients through the turbulent viscosity. The resulting stress tensor can be seen in equation 2.10 below:

$$\tau_{ij} = 2\mu_T S_{ij} - \frac{2}{3}\rho k S_{ij} \quad \ldots.(2.10)$$

The most significant area of focus in this work is the two equation class of models. These models are deemed complete because two transport equations are derived which define two scalars (such as turbulent kinetic energy, energy dissipation or the specific dissipation rate). The Reynolds stress tensor is then computed using an approximation which relates the tensor to the velocity gradients and eddy viscosity (Davidson, 2011). The assumption that is made is dependent on the model being used, as discussed below.

$$V_t = Ul \quad \ldots(2.11)$$

In eddy viscosity models an expression for the turbulent viscosity is wanted, the dimensions of which are [m2/s]. This dimension can be achieved by multiplying a turbulent velocity scale by a turbulent length scale such as

$$l = \frac{k^{\frac{3}{2}}}{\epsilon} \quad \ldots (2.12)$$

Within the eddy viscosity models are two of the most common RANS models, the K-Epsilon and KOmega models. The K-Epsilon and K-Omega models are both two-equation turbulence models, which means two turbulent quantities are solved in the model equations. From the two quantities in each model, a length scale, a timescale and so on can be formed (Pope, 2000). The K-Epsilon model is the most widely used turbulence model where the transport equations for the turbulent kinetic energy and the energy dissipation. These transport equations are used to determine the velocity scale and the length scale of the turbulence (Ferziger & Peric, 2002). The length scale is defined by Davidson (2011) Wilcox defines the turbulent viscosity for the K-Epsilon model as per equation (2.14).

$$\mu_T = \frac{\rho C_\mu k^2}{\varepsilon} \quad \ldots . (2.14)$$

The profile of the turbulent kinetic energy has greater amplitude near the wall than in the mean velocity profile. These peaks (regions of greater amplitude of turbulent kinetic energy) make it difficult to accurately capture the flow data near the wall. To overcome this, a finer mesh needs to be used near the wall. At high Reynolds numbers an insufficient mesh becomes an even greater problem as the viscous sub layer is extremely thin. This is where separate wall functions are introduced to overcome the issue (Ferziger & Peric, 2002). The K-EPSILON model performs reasonably well for two-dimensional thin shear flows where the streamline curvature and mean pressure gradients are both low (De

Beristain, 2012). There are several variations of the K-Epsilon model available in Star CCM+ with the most relevant model being the Realisable K-Epsilon Model.

$$\mu_T = \frac{\rho k}{\omega} \quad \ldots.(2.15)$$

$$\varepsilon = \beta^* \omega k \quad \ldots.(2.16)$$

$$l = k^{1/2}\, \omega \quad \ldots.(2.17)$$

The second most widely used turbulence model is the K-Omega model. Here, the standard turbulent kinetic energy equation is used but is introduced as a length determining equation. In this model is defined as the specific dissipation rate or "the rate of dissipation of energy in unit volume and time" (Wilcox). This property derives its name from its definition. The K-Omega model has the following definitions for turbulent viscosity, energy dissipation and length scale (Wilcox, 1993).

Recalling that the RANS approach also has a second category of turbulence models. These models solve for the Reynolds stress tensor terms rather than the turbulent viscosity term in the averaged Navier Stokes equations. In this category there are the Reynolds Stress Transport (RST) models. The RST models are the most complex turbulence models in Star CCM+. They account for effects such as streamline curvature, rapid changes in strain rate and anisotropy due to swirling motions by solving transport equations for all components of the specific Reynolds Stress tensor. The complexity of the RST models is such that seven additional equations need to be solved in three dimensions as opposed to the two equations of a K-Epsilon model. This makes the RST models computationally expensive and not a very likely option. There are three different RST models in Star CCM+, namely, Linear Pressure Strain, Quadratic Pressure Strain and Linear Pressure Strain Two-Layer (CD-Adapco, 2013).

2.7 Previous Research

Several other studies were examined during the literature review. A few of these are presented below. These works influenced parameters and characteristics of the numerical model designed for the scaled and full size turbopump impellers.

Hellstroom, et al., (2012) modelled the unsteady flow in a radial compressor using the LES technique. The reasoning behind the use of the LES technique was that the flow in the compressor has unsteady large scale structures and separation zones. In the study carried out by Hellstrom et al, no explicit subgrid scale model was used. Instead only numerical dissipation accounts for the sub-grid scale dissipation at the smallest scales (Hellstroom, et al., 2012). Jafarzadeh, et al., (2010) performed a general three dimensional simulation of turbulent flow through a centrifugal pump to predict the velocity and pressure fields. The results were used to form the characteristic curve of the pump which were compared to experimental data and proved to be within an acceptable range. Once the model had been validated the study went on to investigate the effect the number of blades on the impeller had on the efficiency of the pump. Jafarzadeh, et al., (2010) uniquely modelled the impeller as well as the volute, taking into account the interactions between them. Jafarzadeh, et al., (2010) used three different regions in their model, namely, the inlet, the rotating region and the outlet. Each region was discretised independently. The inlet and rotating regions made use of structured grids while the outlet region had a mixture of a structured and unstructured mesh leading to a cell count of 5.8 million cells. Jafarzadeh, et al., (2010) also tested three different turbulence models to find the most suitable one. The models tested were standard KEpsilon, RNG K-Epsilon and RSM. During the validation of the CFD model against the experimental data, RNG K-Epsilon and RSM showed a greater accuracy than the standard K-Epsilon model. Jafarzadeh, et al., (2010) selected RNG K-Epsilon as the most suitable as it has a lower computational time when compared to RSM.

Montomoli, et al., (2010) studied the effect of varying small geometries such as the gaps and fillets. An initial analysis was carried out considering a pre-described value for the fillet radius to underline the high impact of geometrical variations on the flow field. Then, five different fillet radii and three different tip gaps were used to provide an understanding

of geometrical uncertainties. Montomoli et al., (2010) use the traditional two equation K-Omega model stating that it “demonstrates higher performances allowing accurate computations and good stability properties simultaneously”. The work goes on to explain that the revised low Reynolds formulation allows a realistic evaluation of the turbulent boundary layer growth with only a small numerical cost. The numerical model is carried out as a steady state simulation using a mixing plane approach. This work uses a computational mesh consisting of 6.2 million cells. The alterations include changing the outlet angle and passage width of the impeller. As with the majority of the studies the domain consists of three regions, the volute, impeller and outlet pipe. The mesh configuration consists of a structured mesh near the wall to allow greater accuracy in the boundary layer region. At regions away from the wall, an unstructured mesh was used to accurately discretise the complex geometry. This unstructured mesh configuration consists of six sided, pyramid and wedge shaped elements. As already stated, the analysis of flow in centrifugal pumps can be done in a steady or transient state. Shojaeefard et al. state that if the volute has fixed blades the flow is unsteady in nature and should be modelled as such. This is due to the interaction of the impeller and diffuser blades at the impeller outlet. However, if the volute does not have fixed blades the system can be modelled as ‘steady’ by defining a rotating reference frame which is applied to the impeller region. Shojaeefard, et al., (2012) make use of a rotating reference frame (applied to the impeller) while the volute remains in the fixed reference frame. To capture the turbulent effects on the flow field, the study used the K-Omega SST turbulence model because of the models high precision when modelling near wall flow. The boundary conditions used for this particular research consist of a pressure inlet and a mass flow outlet. The turbulence intensity at the inlet was set to 5%, although the authors admit it to be an empirical value. The no-slip condition was applied to the solid boundaries and a surface roughness of 100 μm was set. The study used both water and oil for the numerical simulations. Shojaeefard, et al., (2012) also did a mesh independency study and found the optimum number of mesh elements. The total pressure rise inside the pump and the mean differences of circumferential velocity values were used to evaluate the mesh characteristics of the model. The optimum mesh had been reached when the least number of dependent mesh elements were used and the pressure change was negligible. The authors compared the numerical and experimental

results and found that the average difference percentage in each case was approximately 4% (the highest was 4.06% and the lowest 3.35%) which Shojaeefard, et al., (2012) deemed to be satisfactory.

2.8 Cavitation

Cavitation is a common occurrence in the majority of pumping applications and causes material damage, a decrease in pump performance as well as unwanted vibrations and noise. Cavitation occurs as a result of a local pressure loss in the liquid which causes the liquid to vaporise, in the case of a centrifugal pump, commonly at the inlet to the pump impeller. The vapour bubbles then collapse when the local static pressure increases above the saturation pressure resulting in intense pressure waves that impact and cause material loss on the impeller. The process of cavitation can be described in three stages (Balasubramanian, et al., 2011):

Cavitation is categorised by a dimensionless number known as the cavitation number (equation 2.18). The cavitation number is dependent on the vapour pressure (Psat), the liquid density, the flow pressure (P) as well as the flow velocity (U). As the cavitation number decreases, the probability of cavitation increases (Asnaghi, et al., 2010).

$$P_g = \frac{P - P_{sat}}{\frac{1}{2}\rho_l U^2} \quad \ldots . (2.18)$$

The cavitation number is an important parameter especially when dealing with different operating conditions. A constant cavitation number found despite different operating conditions implies a similar degree of cavitation susceptibility in a given configuration. This means that for two pumps with the same cavitation number, the level of cavitation should be the same relative to the pump size. In the scaling process done by Smyth (2013) the cavitation number was kept relatively similar (0.087 in the full pump and 0.091 in the scaled down case) which means that the degree of cavitation in the three dimensional models of the two pumps should be similar.

Cavitation Patterns

There are several different patterns of cavitation which are defined by the growth of vapour. The interfaces between the liquid and vapour phases hold different shapes which are vital in identifying the type of cavitation present. Some of the cavitation patterns include travelling bubble cavitation, attached cavities, vortex cavitation and shear cavitation which are described below.

Travelling bubble cavitation

Figure 2.3 shows a typical visualization of travelling bubble cavitation on a foil section in a hydrodynamic tunnel. In travelling bubble cavitation, separate bubbles are present which grow on the suction side of the foil. These bubbles are to some extent, similar to the bubbles produced by a boiling liquid on a heated wall.

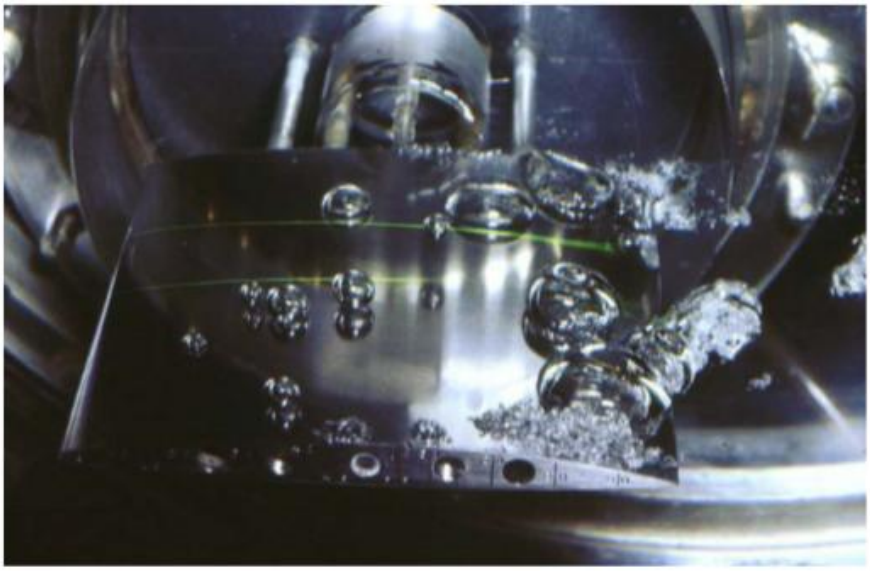

Figure 2.3: Travelling bubble cavitation (Franc, 2006)

This type of cavitating flow shows the weak point in the liquid from which the bubbles are able to form. These weak points are known as cavitation nuclei and are typically microbubbles in the flow. These microscopic bubbles become macrobubbles as the flow passes through a region where the pressure drops below the saturation pressure of the liquid. The bubbles are often not simply spherical in shape as the presence of a wall or

nearby neighbouring bubbles cause deviations from the spherical shape. This configuration has its name as the bubbles are conveyed by the flow over the wall. The bubbles grow in the low pressure region and then collapse in the region of pressure recovery downstream.

Attached cavitation

Attached cavitation the vapour cavity interface is partly attached to a solid surface in a quasi permanent way. Leading edge cavitation (figure 2.4) occurs at low pressure zones of the blade surface and is also known as sheet cavitation when it closely resembles a thin film-like layer on the solid surface. Leading edge cavitation can be partial or appear as super cavitation when the cavity grows sufficiently to envelope the whole body. Leading edge cavitation often occurs in hydraulic machinery that operates under off-design conditions (Franc, 2006) . The cavity interface can either be smooth, glossy and transparent or frothy (similar to that of a highly turbulent boiling surface). In figure 2.4 the detachment is smooth which shows a locally laminar flow which becomes more turbulent downstream.

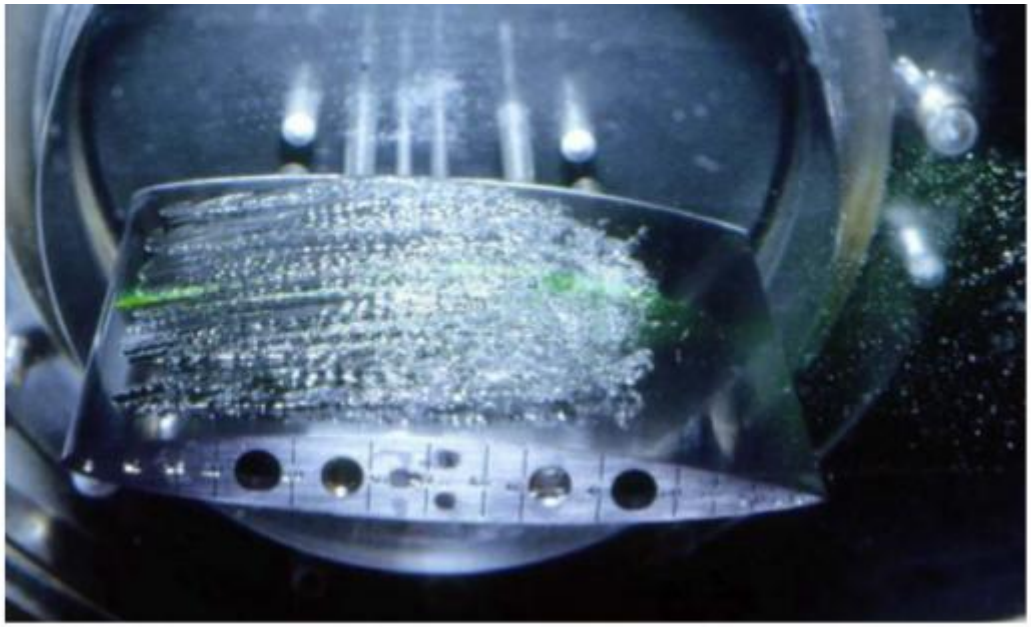

Figure 2.4: Leading edge cavitation (Franc, 2006)

Vortex Cavitation

In the configuration of a 3D hydrofoil the pressure difference between the pressure side and suction side of the hydrofoil produces a secondary flow which goes around the tip and generates a vortex.

This vortex source is at the tip of the foil. The centre of the vortex has the lowest pressure as the centrifugal forces create a higher pressure away from the core. This low pressure region at the vortex core causes the formation of cavitation as seen in figure 2.5.

A common example of vortex cavitation is the cavitation that often occurs on marine propellers where a vortex is produced at the tip of each of the blades as seen in

FIGURE 2.5: VORTEX CAVITATION GENERATED BY A THREE DIMENSIONAL HYDROFOIL

(FRANC, 2006)

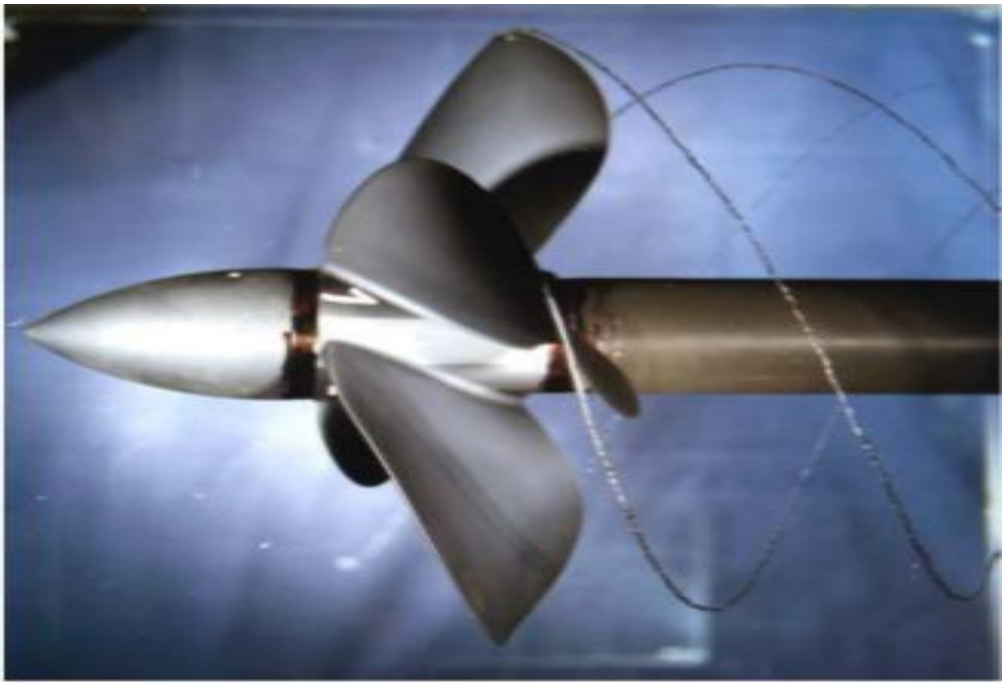

FIGURE 2.6. TIP VORTEX CAVITATION IS USUALLY THE FIRST TYPE OF CAVITATION EXPERIENCED ON MARINE PROPELLERS.

2.9 Cavitation Nuclei

As expressed earlier, there are points in a liquid flow which act as nuclei for the growth of the vapour phase. The most common model of a nucleus is that of a microbubble (Franc, 2006) and a summary of Franc (2006) describes this model below.

Unless a liquid is treated and deaerated, it contains dissolved gas. An example of this is the presence of Nitrogen and Oxygen in tap water. The microbubbles that form when a liquid is subjected to a low pressure contain non condensable gas (such as nitrogen and oxygen) as well as vapour.

Thermodynamic equilibrium is assumed at the interface of the microbubble. This equilibrium requires that equation (2.19) is satisfied, where Pg represents the partial pressure of the gas in the bubble and Pv is the partial pressure of the vapour in the bubble which is assumed to be equal to the vapour pressure of the liquid (Franc, 2006). is the

pressure of the liquid flow while S represents the surface tension on the bubble and R is the radius of the microbubble.

$$P_g + P_v = P_\infty + \frac{2S}{R} \quad \ldots.(2.19)$$

When looking at the bubble formation there is a link between the critical radius and the pressure. A nucleus is characterised by the mass of non-condensable gas. This mass is assumed constant irrespective of the evolution of the nucleus because the assumption means the transfer of mass through the interface of the microbubble (via diffusion) can be ignored.

$$P_g = \frac{K}{g^3} \quad \ldots.(2.20)$$

Franc states that the constant K is characteristic of the considered nucleus. Equation (2.20) can be rewritten by substituting equation (2.19) to produce equation (2.21).

$$\frac{K}{R^3} + P_V = P_\infty + \frac{2S}{R} \quad \ldots.(2.21)$$

For any nucleus with the characteristic K, equation (2.21) allows for the computation of the equilibrium radius (R) for any pressure of the flow. This can be seen from the equilibrium curve (figure 2.7) which is generated from equation 2.21. The equilibrium point has a minimum point defined by a critical radius and a critical pressure which can be denoted as:

$$P_e = P_v - \frac{4S}{3RC}$$

$$R_C = \sqrt{\frac{3K}{2S}} \quad \ldots.(2.22)$$

If a nucleus at point 2 on the curve experiences a pressure decrease that takes the pressure below that of the critical pressure (pc), the nucleus will grow indefinitely without reaching a new equilibrium. As with the previous case of point 3, the nucleus here will form a cavitation bubble. The Pc value can therefore be seen as a critical value, below which the nucleus will grow indefinitely, become destabilised and form a bubble.

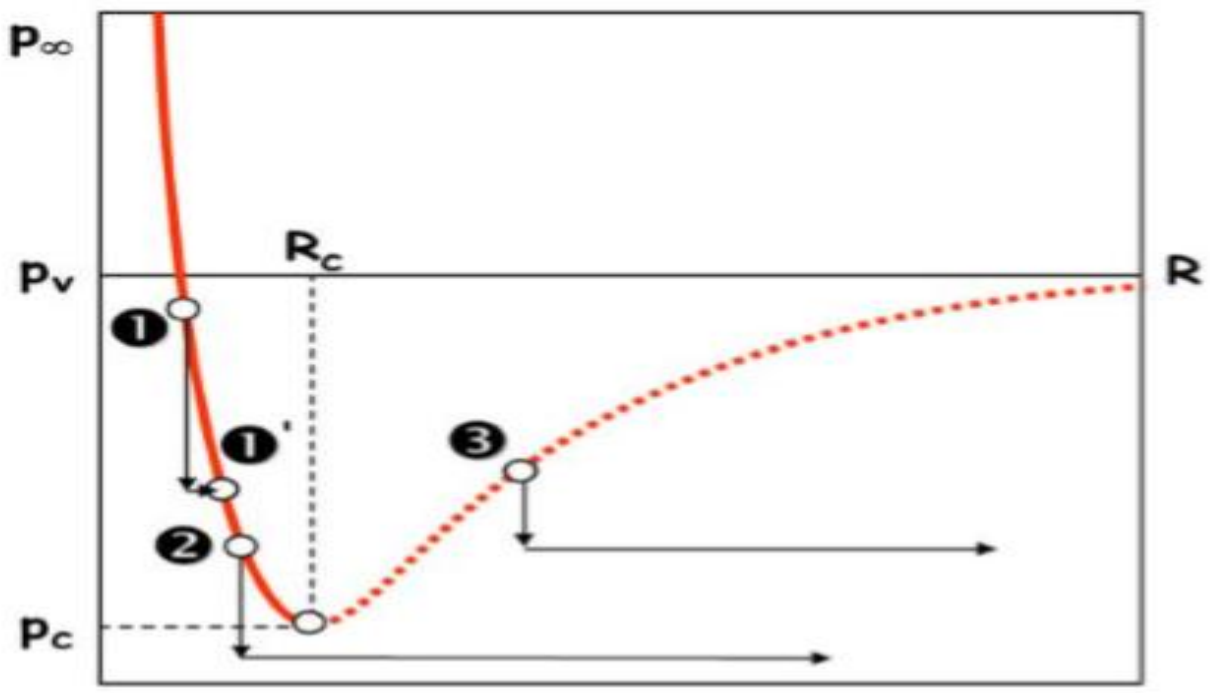

Figure 2.7: Equilibrium radius of a nucleus as a function of pressure

(Franc, 2006)

The above model shows that the critical pressure for the onset of cavitation is slightly lower than the vapour pressure. The model also shows that the smaller the nucleus radius is, the greater the deviation from the vapour pressure. This delay in the start of cavitation is due to the surface tension (Franc, 2006). Despite this, the critical pressure is often taken as the vapour pressure of the liquid. Franc explains that in a liquid where a large variety of nuclei exist, it is common practice for the pressure at which cavitation will form to be taken as the critical pressure of the largest nuclei. It can be seen from the discussion above (and equation 2.22) that the larger the nuclei is, the closer the critical pressure is to the vapour pressure. While it is generally acceptable to take the vapour

pressure as the starting point of cavitation, this model shows that deviations can be expected depending on the liquid quality in terms of nuclei content.

2.10 Cavitation Modelling

To model cavitation in Star CCM+ one needs to recognise that cavitation is classified as a multiphase flow as it consists of both liquid and vapour simultaneously. In multiphase flow, distinct interfaces exist between the different phases which mix on a macroscopic scale. There are two distinct categories of multiphase flow, dispersed flow and stratified flow. Cavitation falls into the dispersed flow category. For these two flow types, Star CCM+ offers five different models (CD-Adapco, 2013) to best suit the application at hand, namely:

The Multiphase Segregated Flow model: also known as the Eulerian Multiphase model, it solves conservation equations (for mass, momentum and energy) for each phase. Phase interaction models are present to allow the influence of one phase on another to be modelled. The Lagrangian Multiphase model: solves the equations of motion for parcels of the dispersed phase as they travel through the system. It is best suited to systems that consist mainly of a single continuous phase which has a relatively small secondary phase volume (droplets/bubbles). It also deals well with modelling the interaction of the discrete phase with physical boundaries. The Discrete Element model (DEM): is an expansion of the Lagrangian model. The main difference being that here individual particles are modelled instead of representative parcels, as in the Lagrangian model. The Fluid Film model: using boundary layer approximations as well as velocity and temperature profiles of a fluid film, this model predicts the dynamic characteristics of wall films. Film motion is predicted using thin shells located on the surface of solid walls on which the film is formed. The volume of fluid (VOF) model: is used in flows that have two (or more) immiscible fluid phases, where each phase contributes a significant structure within the flow. This model captures the motion of the interface between phase.

The seed based approach consists of two interacting phases, liquid and gas, with positive mass transfer from liquid to gas. The volume fraction of gas is described as:

$$\alpha_g = \frac{V_g}{V} = \frac{V_g}{V_g + V_t} \quad \ldots.(2.23)$$

The gas phase in each control volume is assumed to be in the form of bubbles which each have the same radius. The number of bubbles per unit volume is denoted as . This yields the following relationship between the phases:

$$V_g = n_o V_l \frac{4}{3} \pi R^3 \quad \ldots.(2.24)$$

Making the volume fraction of gas:

$$\alpha_g = \frac{n_o \frac{4}{3}\pi R^3}{1 + n_o \frac{4}{3}\pi R^3} \quad \ldots.(2.25)$$

This allows the gas bubble radius to be prescribed as:

$$R^2 = \frac{\alpha_g}{n_o \frac{4}{3}\pi(1 - \alpha_g)} \quad \ldots.(2.26)$$

The mass transfer rate can then be described by the following equation:

$$m = n_o \alpha_l 4\pi \rho_g R^2 \frac{D_R}{D_t} \quad \ldots.(2.27)$$

The liquid therefore vapourises with a volume rate of:

$$V_l = -\frac{m}{\rho_1} \quad \ldots.(2.28)$$

This factor is modelled using the Rayleigh Plesset (RP) equation which describes the development of the bubble radius when the bubble lies in an infinite domain. The

equation represents the equilibrium of stress at the interface of the bubble. To obtain the RP equation, the mass and momentum conservation equations in both fluid and gas are considered and the stress equilibrium is then prescribed (Liuzzi, 2012). The RP equation takes into account the inertia, viscous and surface tension effects and can be seen in equation 2.29 where is the liquid viscosity and is the surface tension.

$$R\frac{d^2R}{dt^2} + \frac{3}{2}\left(\frac{dR}{dt}\right)^2 = \frac{\rho_{sat} - \rho_{\infty}}{\rho_l} \qquad \ldots.(2.29)$$

. The main aim of Zhu & Chen, (2012) was to further understand the cavitation suppression mechanism of the gap structure impeller. The gap structure impeller consists of a regular rotor with small blade introduced on the suction side of the regular blades. To further understand this mechanism, Zhu and Chen analysed the cavitation characteristics in a low specific speed centrifugal pump. Zhu and Chen predicted the cavitation performance of two centrifugal pumps and compared them with experimental data which showed a good agreement of results.

O-type grid technology as well as local mesh refinement were used to control the near-the-wall mesh which ensured the requirements of the corresponding turbulence models. The turbulence model that was used was K-Epsilon SST with automatic near wall treatment. Zhu and Chen explain that this model can automatically switch from wall functions to a low Re near wall formulation as the mesh is refined.

2.11 Pump Scaling Laws

The scaling laws had been used by Smyth (2013) to reduce the massive power consumption of the original impeller, to that required to drive a smaller, similar impeller according to the power available and the laboratory test rig. The smaller impeller, which is to be tested experimentally, would then allow the conclusions from the experimental testing to be useful, providing the scaled impeller retained the same operating characteristics as the original impeller

The scaling process looked at the affinity laws described below which are based on the Buckingham Pi Theorem (Smyth, 2013):

$$\frac{Q_a}{Q_b} = \frac{N_a SF^3}{N_b} \quad \ldots (2.30)$$

$$\frac{H_a}{H_b} = \left(\frac{N_a SF}{N_b}\right)^2 \quad \ldots (2.31)$$

The first affinity law ensures that the inlet flow coefficient is kept constant and determines the flow rate (Qb) for the scaled pump. The second law was used to calculate the head rise (Hb) across the scaled pump while ensuring that the head coefficient remains constant between the pumps.

To be useful, a scaled item must be geometrically similar, kinematically similar and dynamically similar (Fox, et al., 2010). The first (geometric similarity) is obvious in that the scaled object should have the same shape as the original model. The linear dimensions of the scaled object should correspond to the original model through a constant scale factor. Naturally this is difficult with objects as complex and turbomachinery.

CHAPTER 3

METHODOLOGY

STEP TO DESIGN IN ANSYS-

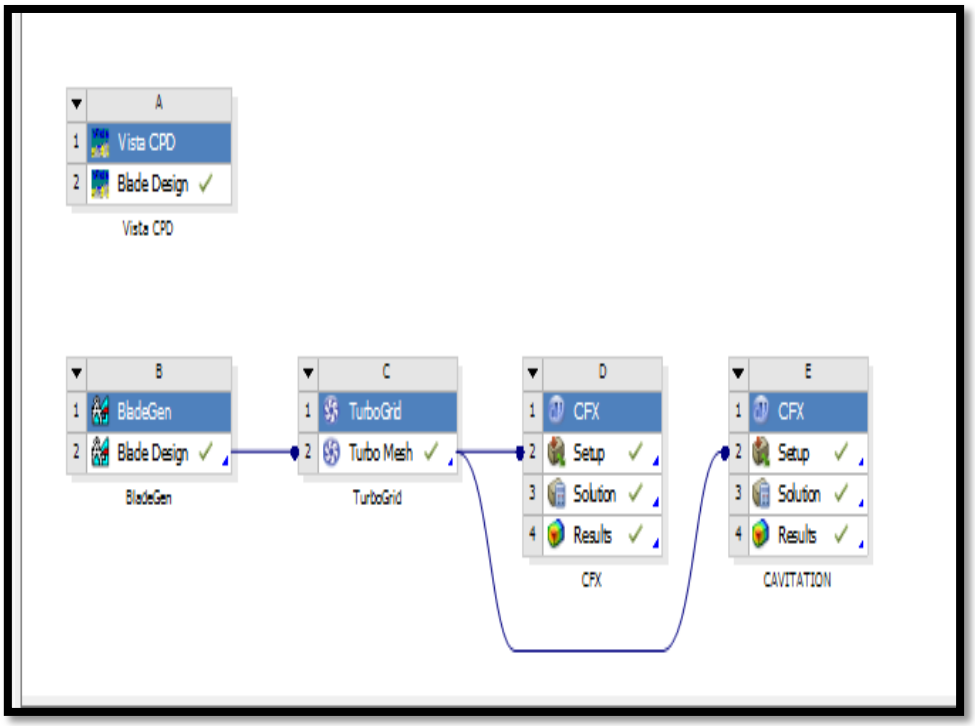

FIGURE 3.1 WORK BENCH 18.2 VARIOUS STEP TO DESIGN

Click on vista CPD given in right side of table, double click on blade design and add values then click calculate, you can see the size of plate , you can change size of plate by going to geometry as per your requirement, click automatic design plate if you don't have much data.

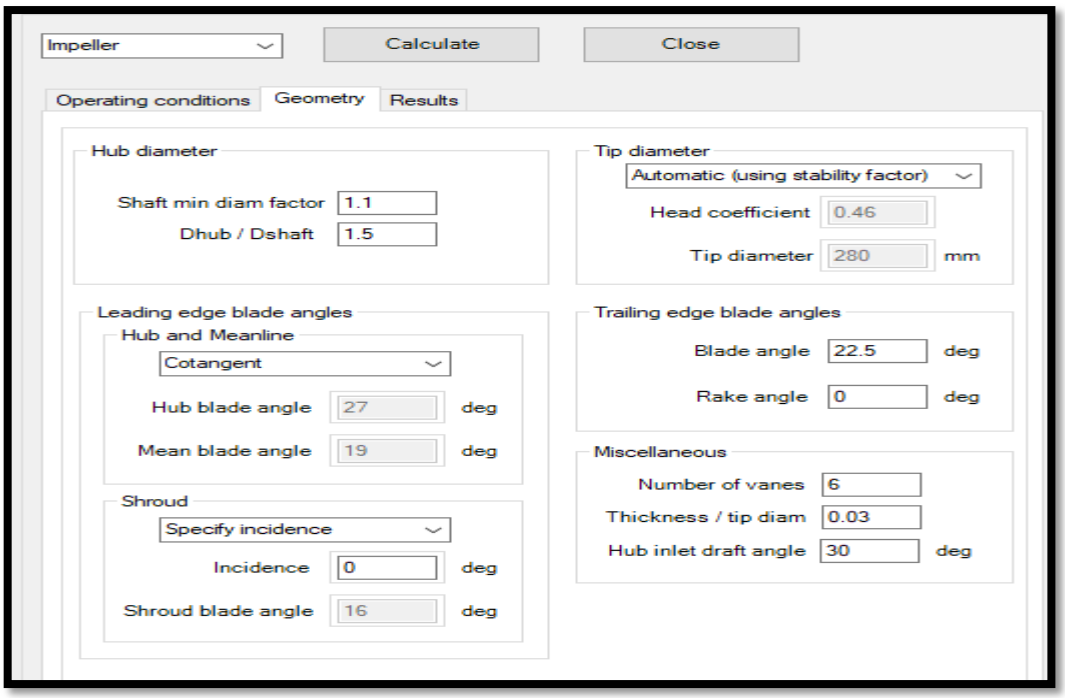

FIGURE 3.2 IMPELLER GEOMETRY

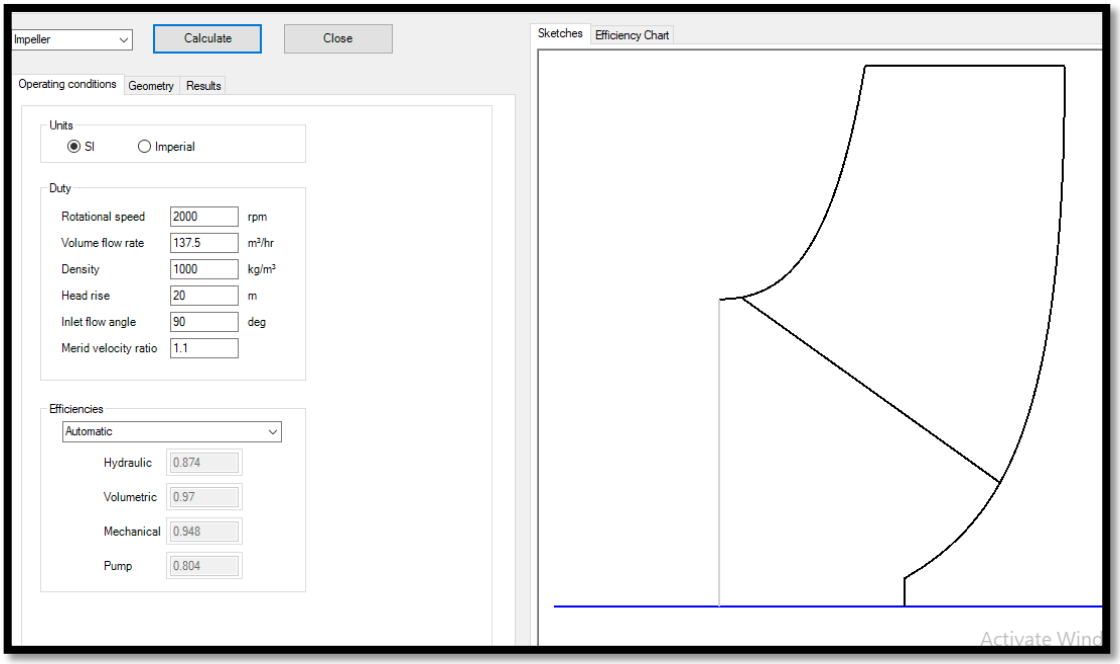

FIGURE 3.3 OPERATING CONDIATION

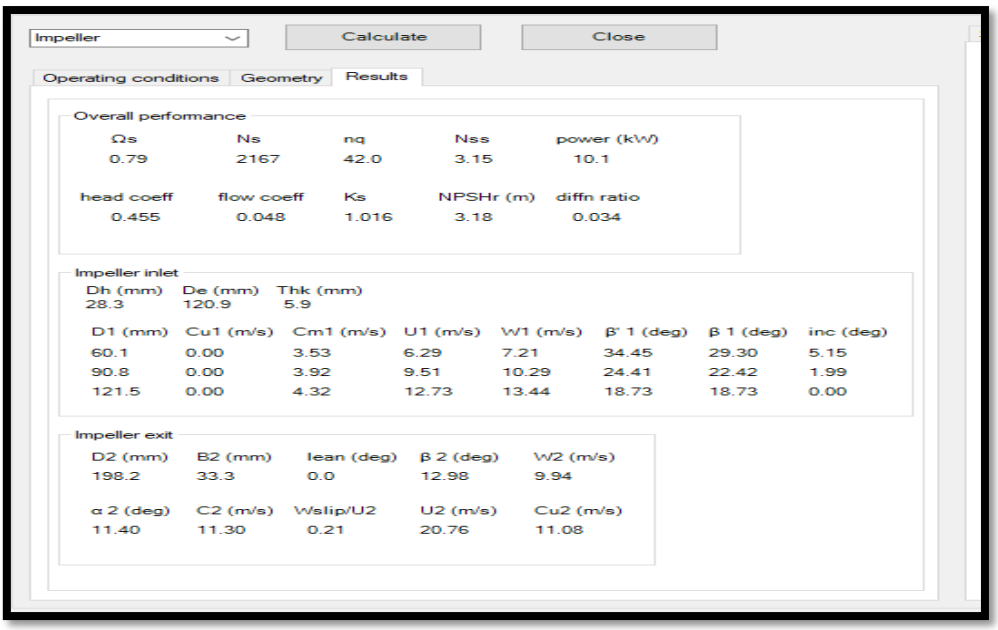

FIGURE 3.4 RESULT OF IMPELLER

Right click on blade design go to create new option and select blade gen option, double click on blade gen design, click 3 d view option and check the view of blade group.

Effect of centrifugal pump if RPM change –If we increase RPM of pump width of plate increases and length of plate decrease and vice versa. Same effect if we change volume flow rate i.e. if we increase volume flow rate width of plate increases and lengh of plate increases and vice versa, if we increase volume flow rate then volume of volute increases and vice versa.

Centrifugal pump and centrifugal compressor both are different. In centrifugal pump fluid is incompressible like water and considered than every fluid flowing through these pump is incompressible but in centrifugal compressor fluid is compressible like air, we always consider fluid in centrifugal compressor as incompressible.

Right click on blade design and transfer the data to turbo grid option, right click on turbo grid and send date to cfx, ensure that outer domain option is turn off in properties of turbo grid, if it not turn off resut will not show properly, right click on turbo mode and

update it.

Now open setup by double click on setup, click on tool option and click on turbo mode option, select machine type as pump,(if your fluid is compressible then choose

compressor), click next, select R_1, go to available volume and expand it, select passage, go to the RPM and add value as 2000, right click on component then add component as S_1, select component type as stationary, select volume type as B-75 click NEXT, select P-TOTAL and INLET MASS FLOW RATE OUTLET.

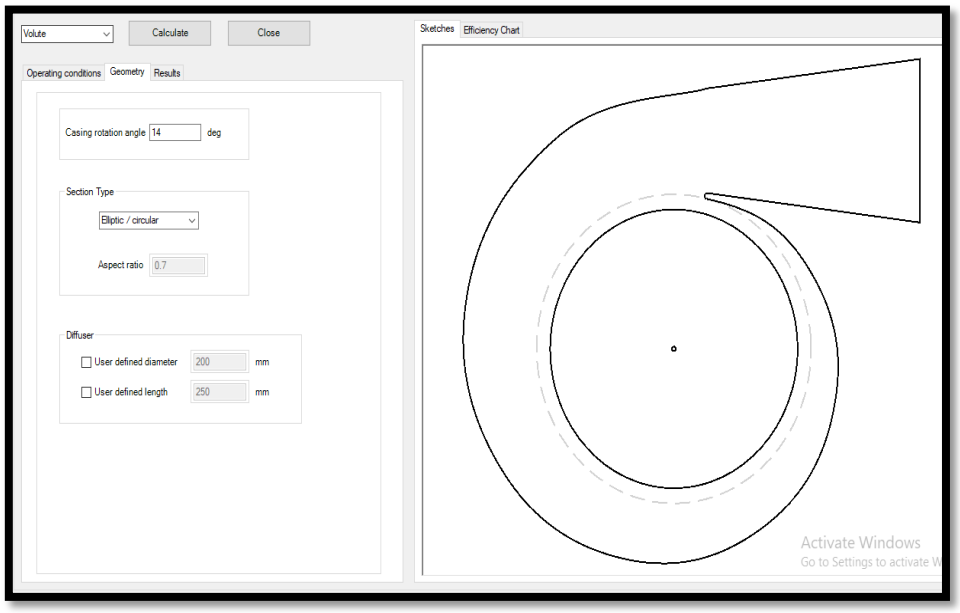

FIGURE 3.7 VOLUTE GEOMETRY

Mass flow rate as 0.5 kg/ sec, Mass flow - per component, Fluid water – Next again click on Next then Next, Go to solver control, Maximum iteration as 200, Click on apply and close, Double click on solution, Run Mode – INTEL MP1 LOCAL PARALLEL PARTITION, Start Run, Go to the result , Click streamline, select the streamlone 1 and observe the flow, stop the animation and cancel it, start from R_1 to R_2 periodic, cick apply.

Go to setup double click on default domain, in fluid and fluid definition add material as water and material as water, reference pressure 0 atm, angular velocity as -2500 rev/ min, go to fluid model, select shear stress transport turbulence then click apply then ok.

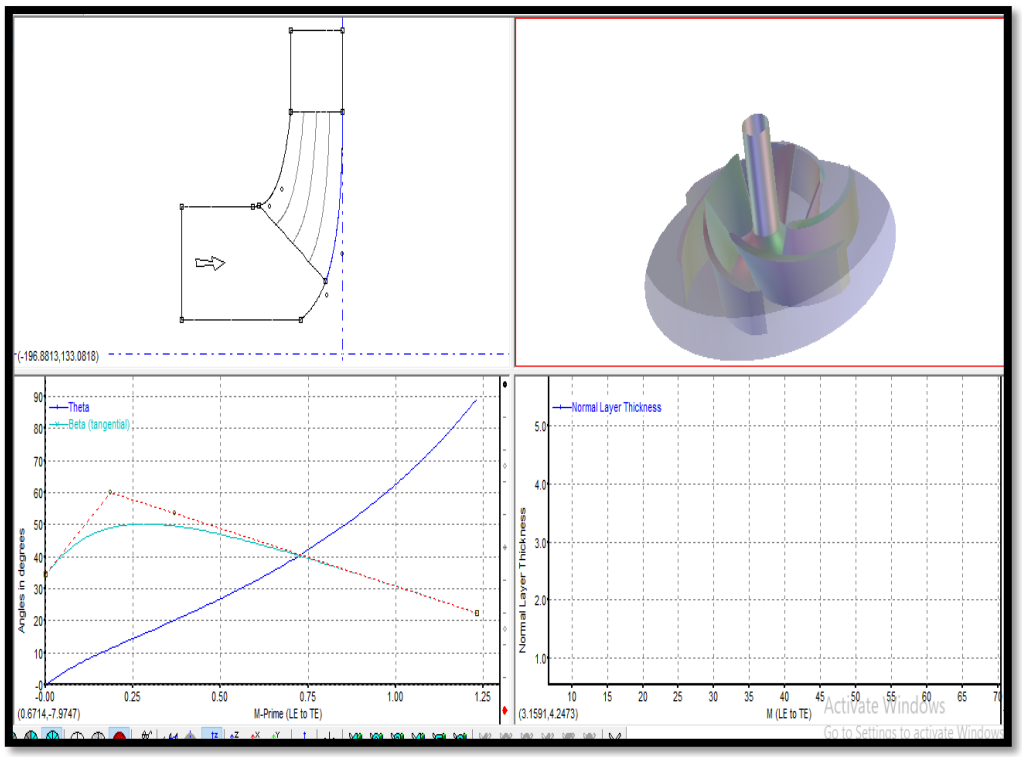

FIGURE 3.6 BLADE GENERATION

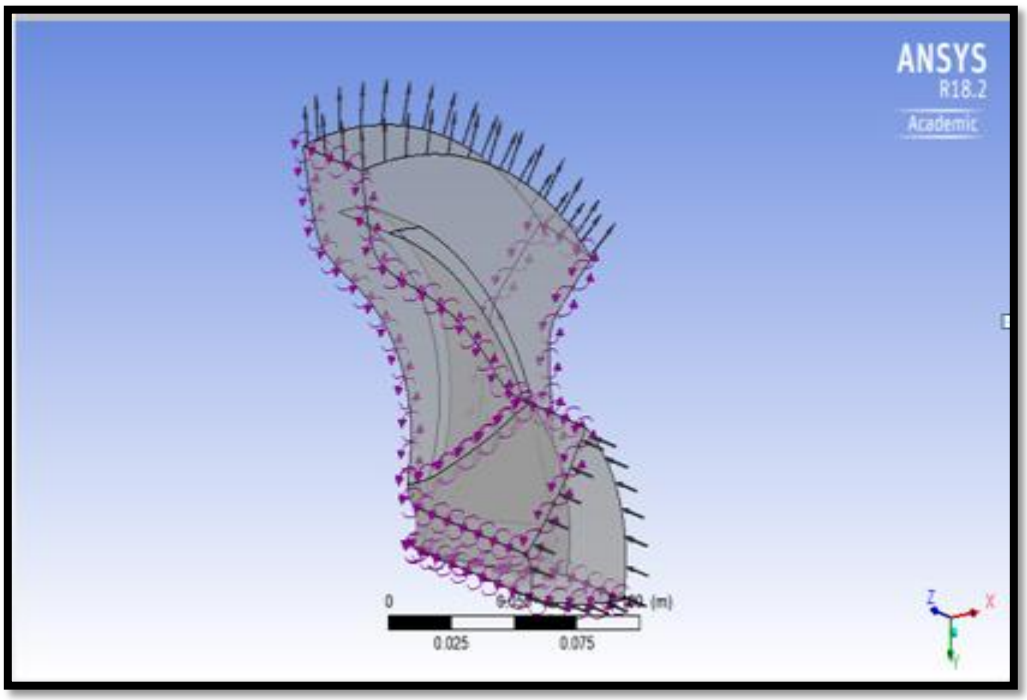

FIGURE 3.7 SETUP

Add boundaries in default domain by right click ok default boundary click on inert then boundaries add inlet, outlet, rotation, fixed, select location as inlet and select stat. frame tot. pressure in boundary detail, add reference pressure as 700000 Pa then click apply ok, in outlet location is outlet, mass flow rate is 35 kg/sec in boundary detail, in rotation boundary type as wall, location is blade, top, bottom, in fixed boundary type is also wal and location is fixed, click on select wall velocity in boundary detail. Double click on water and click on material property change density as 1000 kg/m^3 then click ok, go to the solver control then turbulence numerics select high resolution change no of iteration as 1000, change length of scale as aggressive residual type, click on rotation type ok, double click on rotation then color change mode as variable and range as local, update the project.

CAVITATION

Click on task bar and add duplicate and name it as cavitation, click on setup add material as vapour at 25 ^0C from water data, select management model in fluid model, go to saturation pressure and add value 3170 Pa, add bulk flow rate in as 35 kg/m^3 , in fluid value option volume fraction is 0 for vapour and 1 for water hen click ok, double click on outlet, click option static pressure add value 250000 Pa then ok, save the project and update it, go to solution option click location, select location as volume method, above value in Isovolume mode, vapour fraction in variable and 0.5 in value and click apply change rendering transparency as 0.8

CHAPTER 4

RESULT AND DISCUSSION

Observed Data & Related Graphs

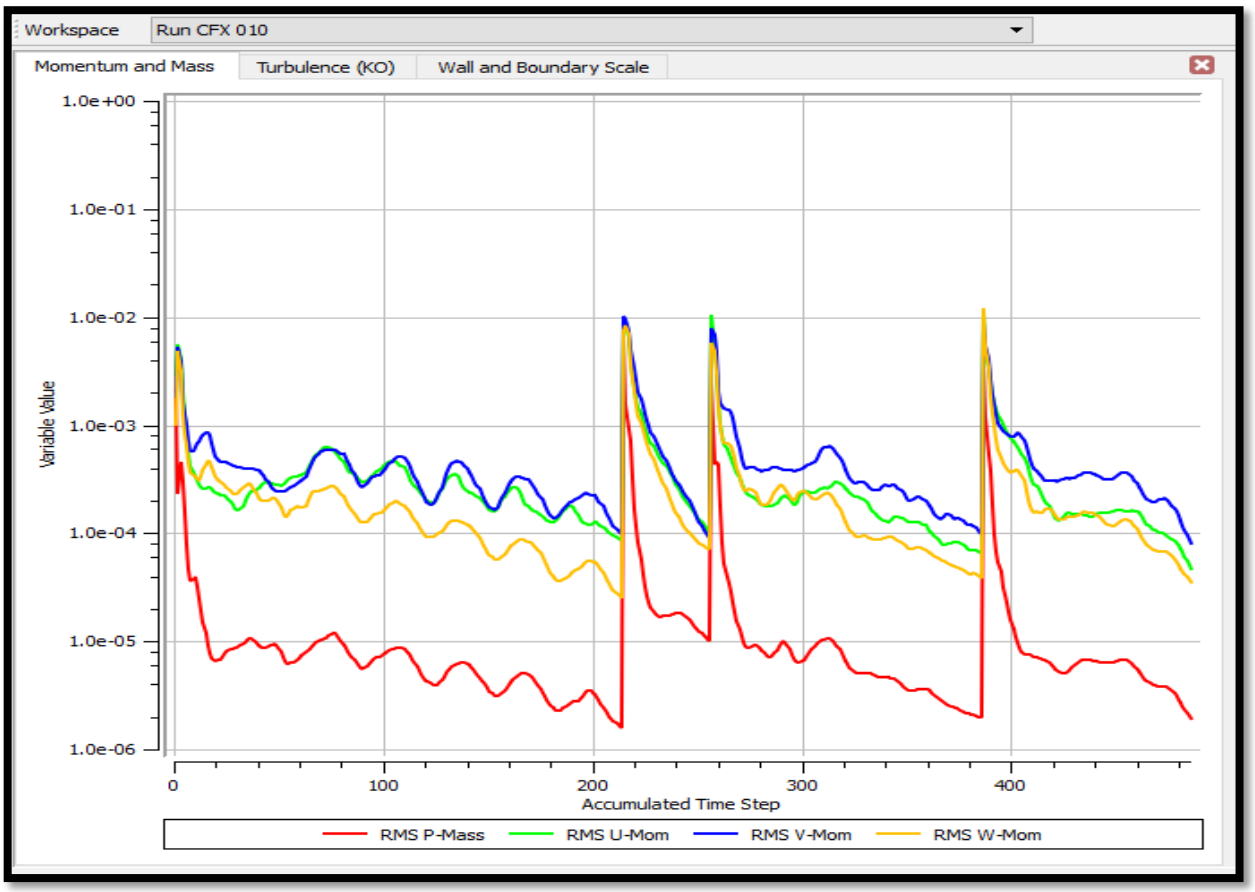

FIGURE 4.1 MOMENTUM CURVE

Figure 4.1 shows iteration and difference of two sloution

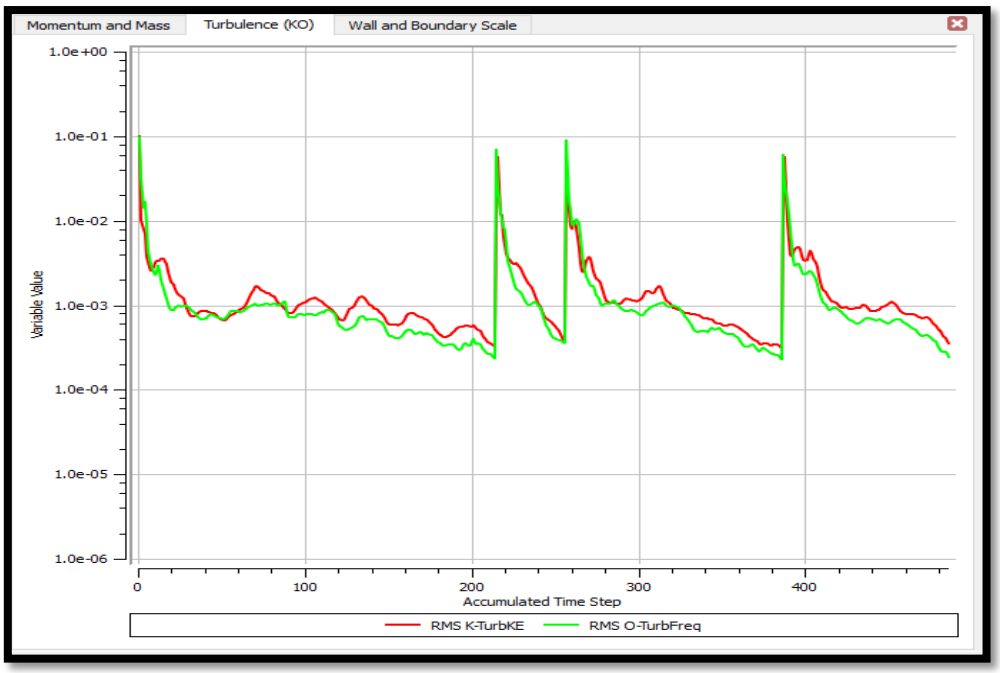

FIGURE 4.2 TURBULANCE CURVE

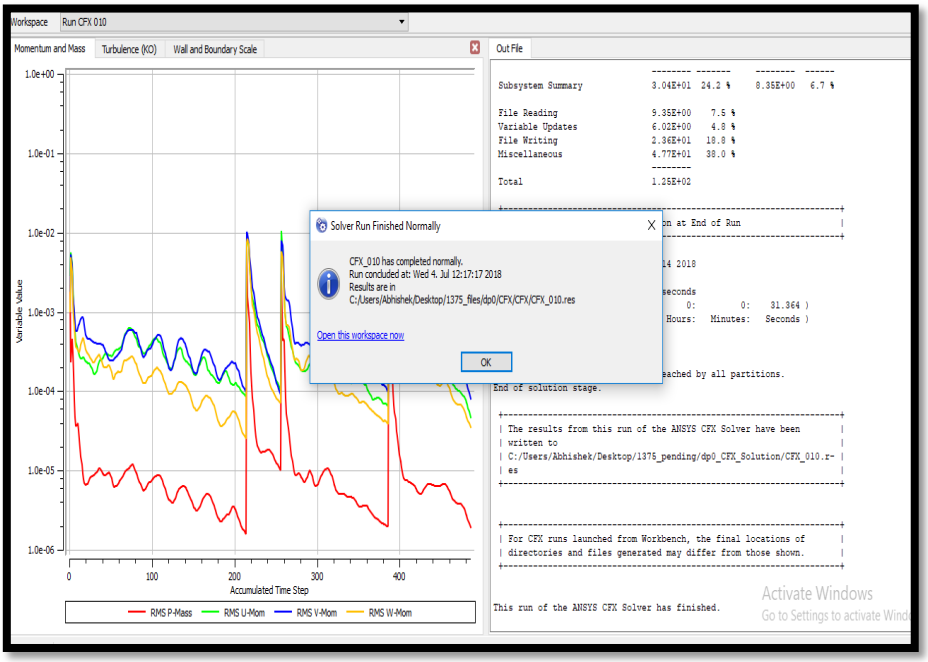

FIGURE 4.3 SOLUTION

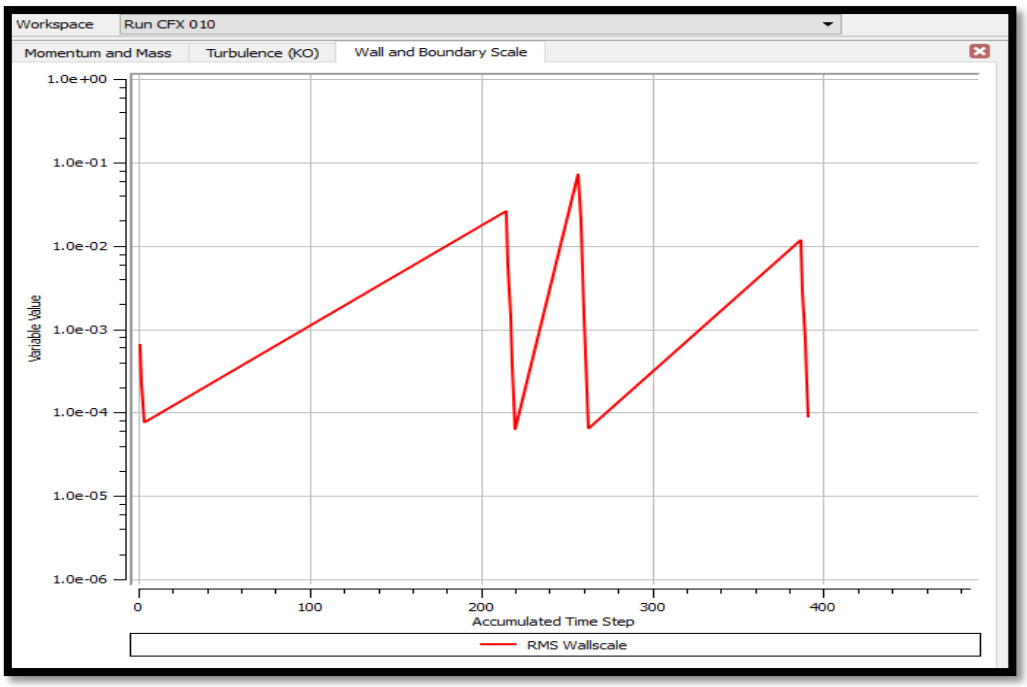

FIGURE 4.4 WALL AND BOUNDARY SCALE

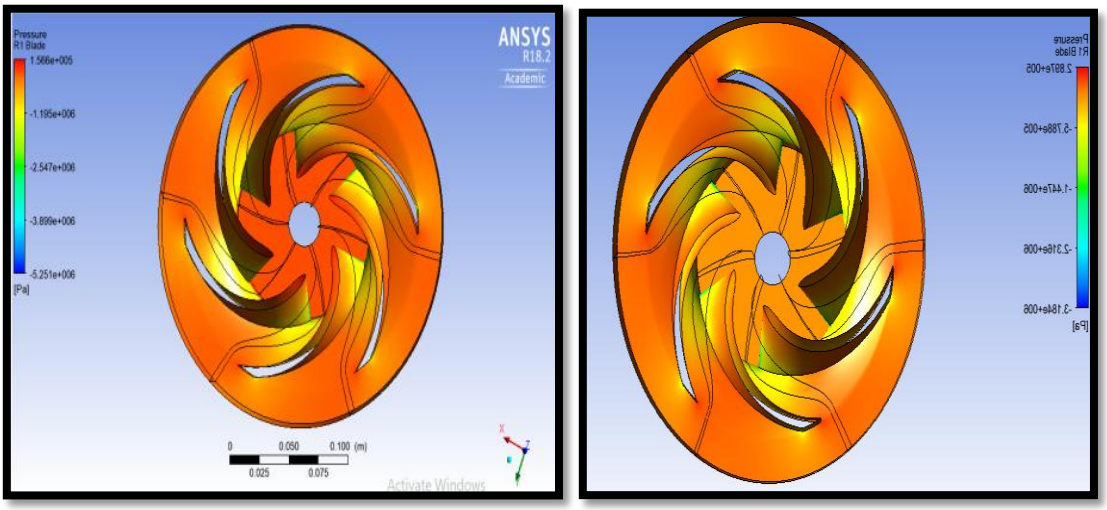

FIGURE 4.5 PRESSURE DISTRIBUTION

Figure 4.5 cavitational pressure is maximum at inner surface and at tip of blade

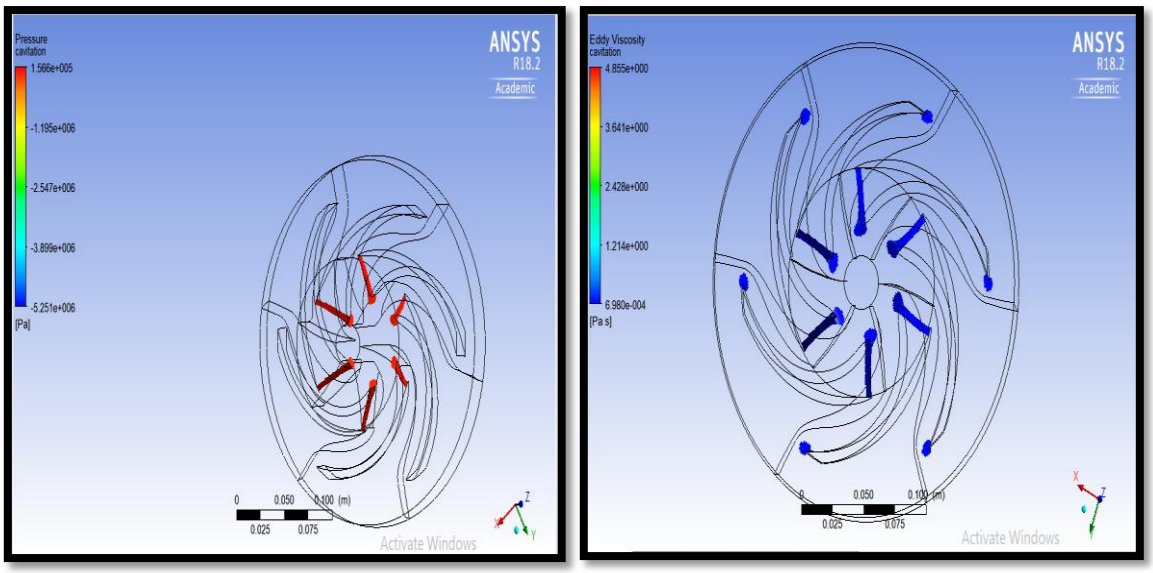

FIGURE 4.6 CAVITATION PRESSURE DISTRIBUTION AT LOW DISCHARGE (75 m^3/hr LEFT HAND SIDE AND 100 m^3/hr RIGHT HAND SIDE)

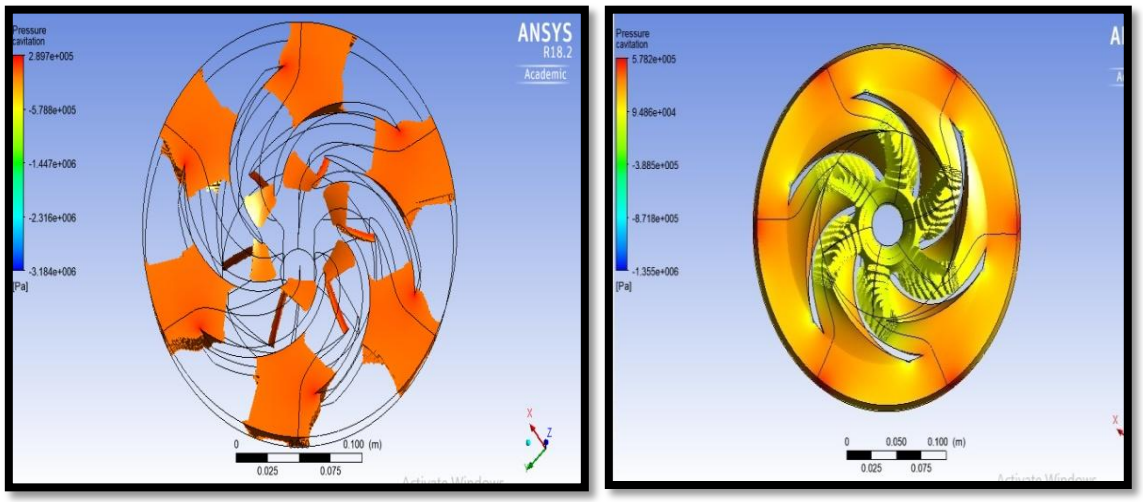

FIGURE 4.7 CAVITATION PRESSURE DISTRIBUTION AT HIGH DISCHARGE (150 m^3/hr LEFT HAND SIDE AND 200 m^3/hr RIGHT HAND SIDE)

Figure 4.6 and 4.7 shows that at lower discharge cavitation, cavitation pressure and area is lower and vise versa

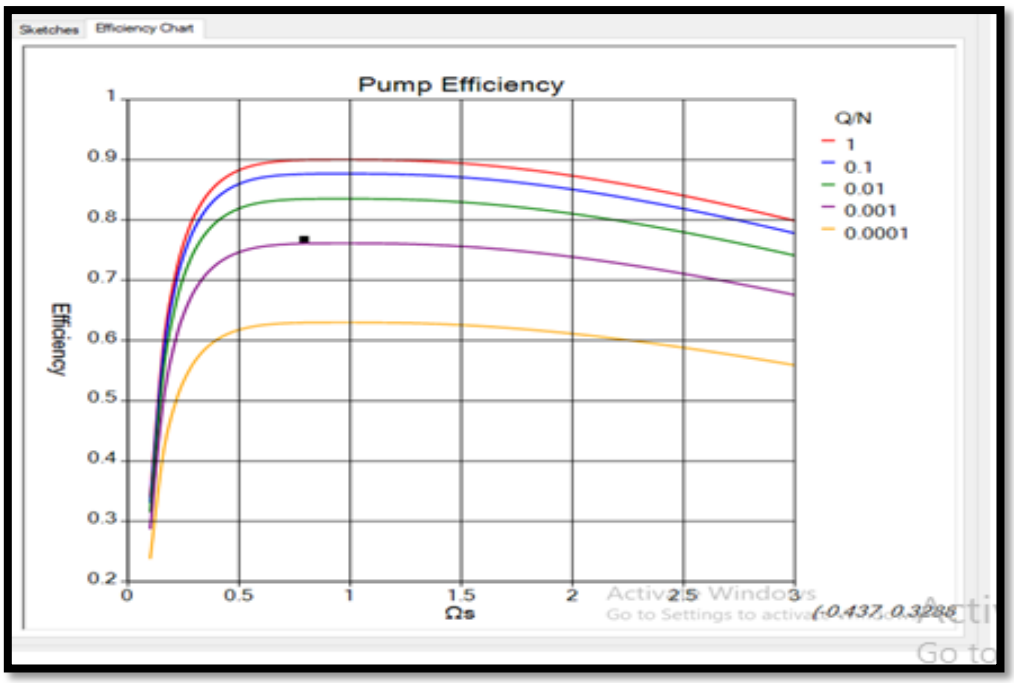

FIGURE 4.8 EFFICIENCY GRAPH OF IMPELLER

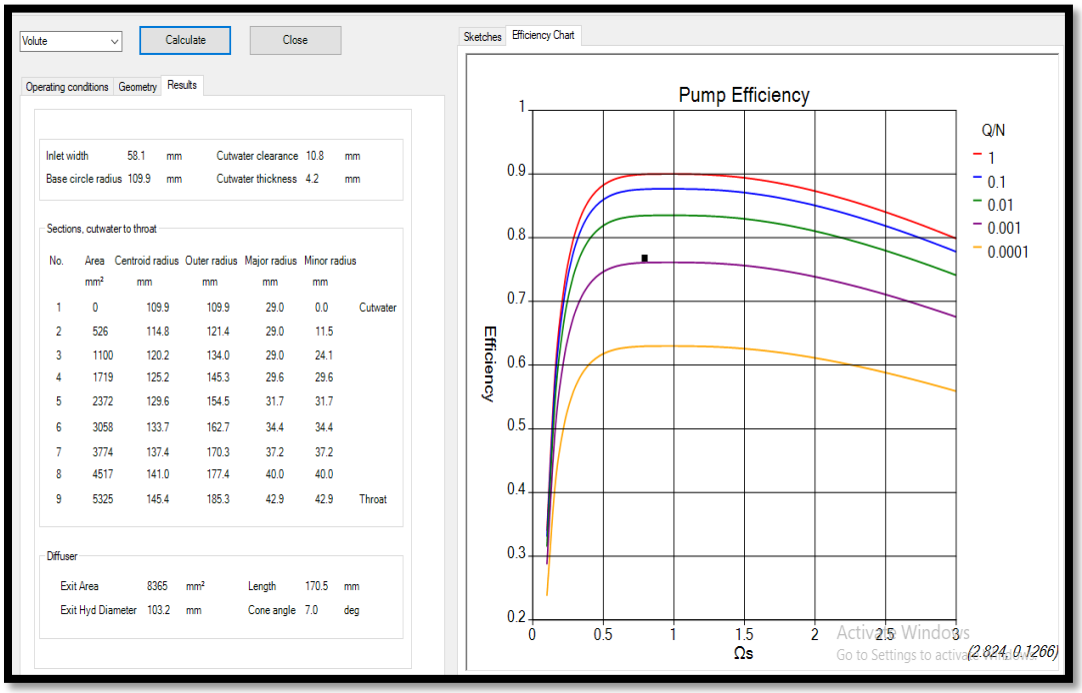

FIGURE 4.9 RESULT AND EFFICEINCY CUREVE OF VOLUTE

TABLE 4.1 DISCHARGE VS CAVITATION AT CONSTANT RPM 2000

DISCHARGE (in m^3/hr)	75	100	112.5	125	137.5	150	162.5	200
CAVITATION (in 10^5 Pa)	1.024	1.566	1.825	2.267	3.608	5.782	8.124	15.558

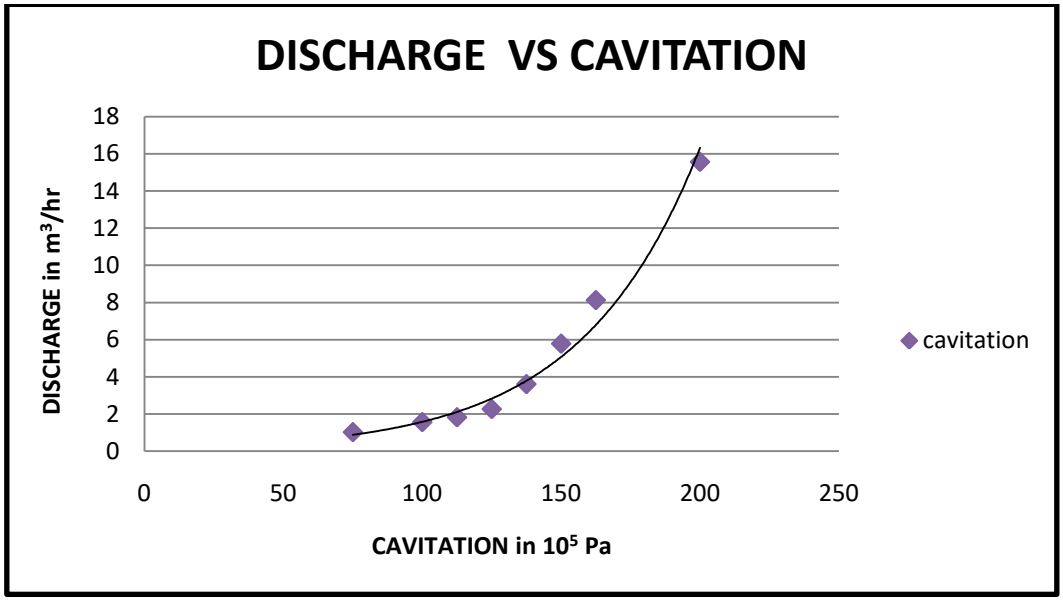

FIGURE 4.10 DISCHARGE VS CAVITATION CURVE

(Figure 4.10 shows that as discharge increases cavitation decreases)

TABLE 4.2 CAVITATION VS R.P.M. AT CONSTANT DISCHARGE 137.5 m^3/ hr

RPM	2000	1750	1500	1250	1000
CAVITATION (10^5 Pa)	2.897	5.304	6.341	7.254	9.255

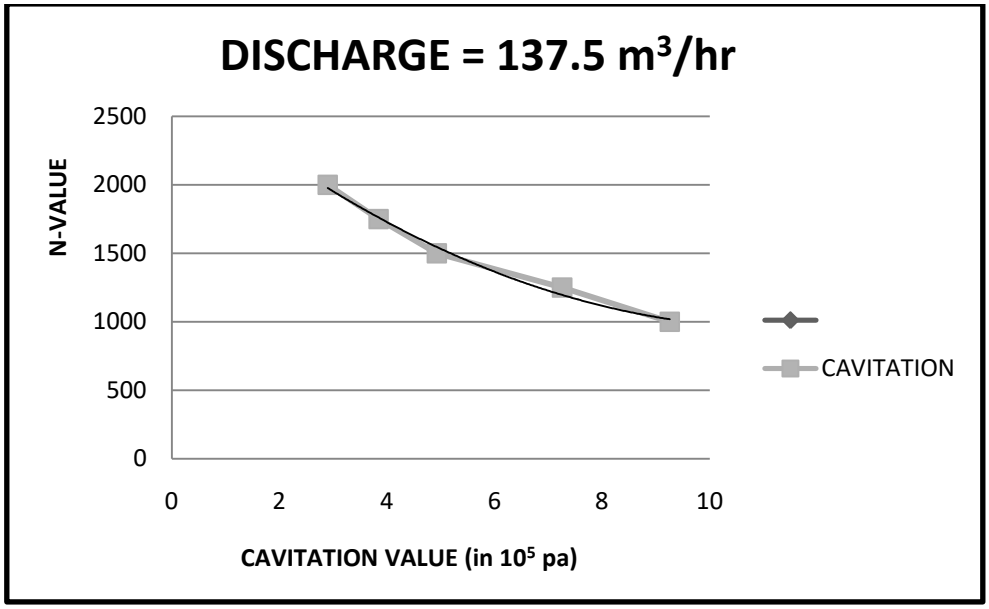

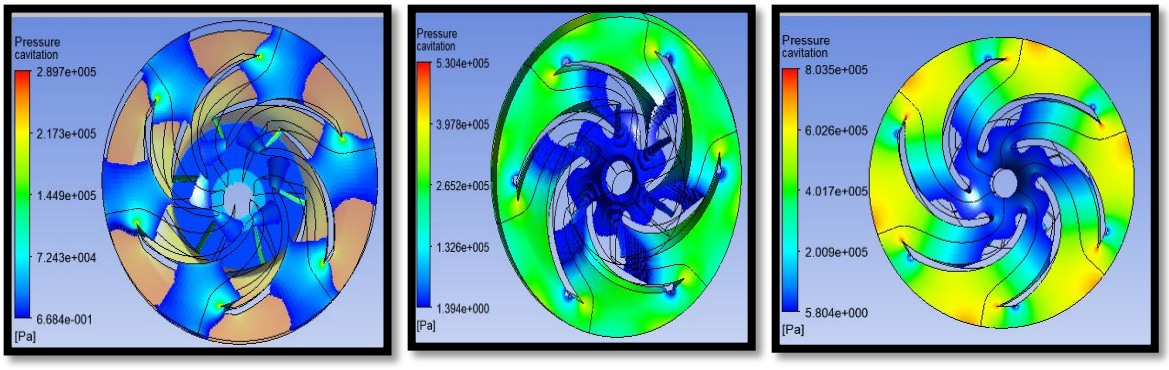

RPM = 2000 **RPM = 1750** **RPM = 1500**

FIGURE 4.11 SHOWS CAVITATION IN CENTRIFUGAL PUMP AT VARIOUS R.P.M. AT CONSTANT DISCHARGE OF 137.5 m^3/hr

TABLE 4.3 CAVITATION VS R.P.M. AT CONSTANT DISCHARGE 125 m^3/ hr

R.P.M.	2000	1750	1500	1250	1000
CAVITATION (in 10^5 Pa)	2.062	4.821	7.317	9.369	18.264

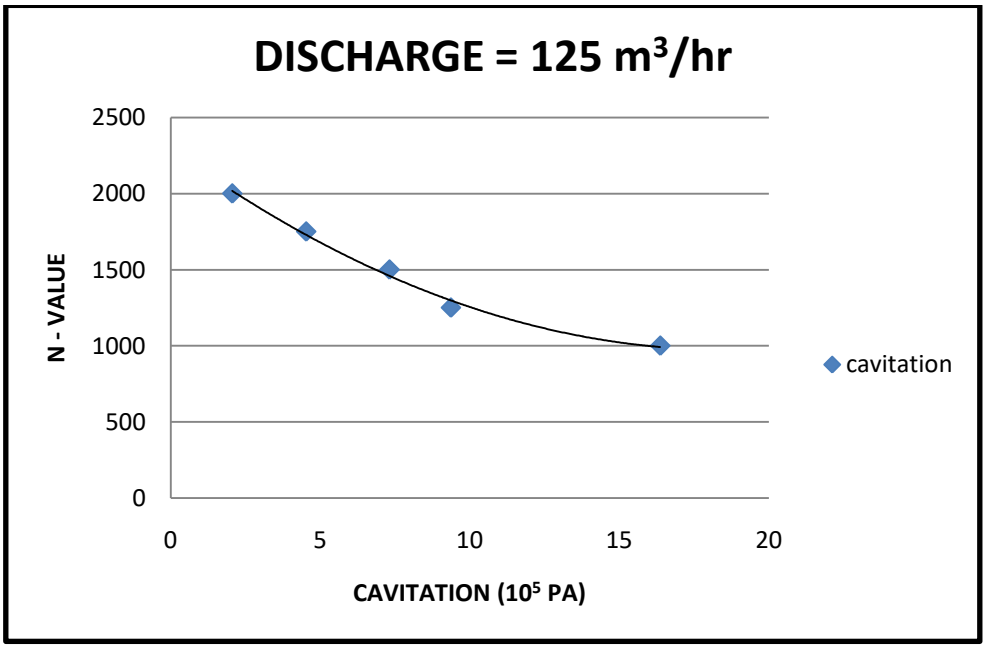

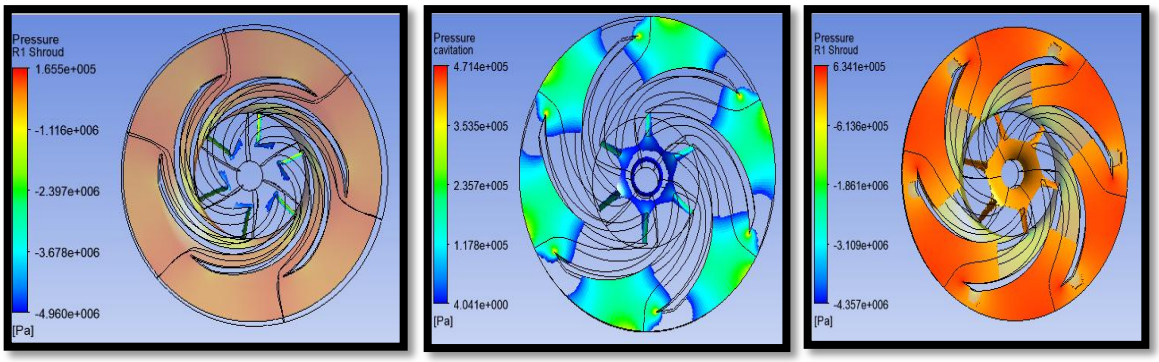

RPM = 2000 **RPM = 1750** **RPM = 1500**

FIGURE 4.12 SHOWS CAVITATION IN CENTRIFUGAL PUMP AT VARIOUS R.P.M. AT CONSTANT DISCHARGE OF 125 m^3/hr

TABLE 4.4 CAVITATION VS R.P.M. AT CONSTANT DISCHARGE 112.5 m^3/ hr

R.P.M.	2000	1750	1500	1250	1000
CAVITATION (in 10^5 Pa)	1.566	3.262	6.341	11.452	18.207

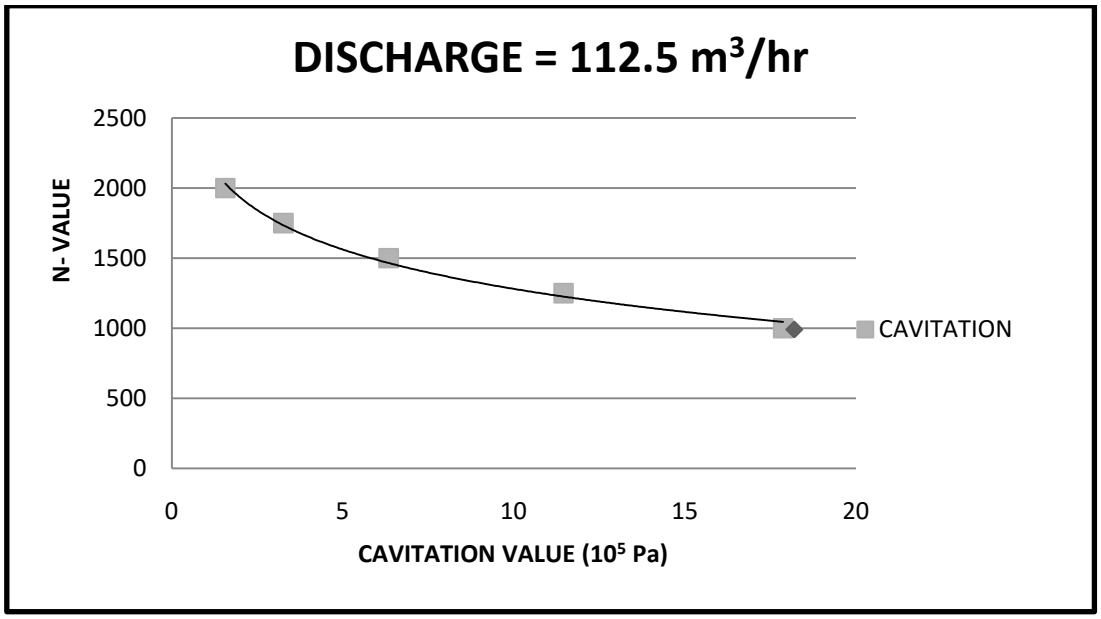

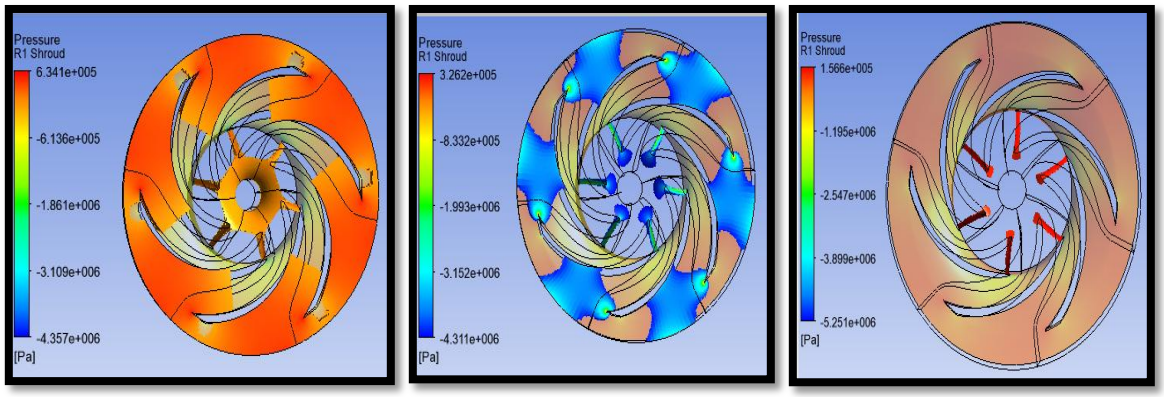

RPM = 2000 **RPM = 1750** **RPM = 1500**

FIGURE 4.13 SHOWS CAVITATION IN CENTRIFUGAL PUMP AT VARIOUS R.P.M. AT CONSTANT DISCHARGE OF 112.5 m^3/hr

TABLE 4.5 CAVITATION VS R.P.M. AT CONSTANT DISCHARGE = 100 m^3/hr

R.P.M.	2000	1750	1500	1250	1000
CAVITATION (in 10^5 Pa)	1.629	1.835	4.714	6.358	12.446

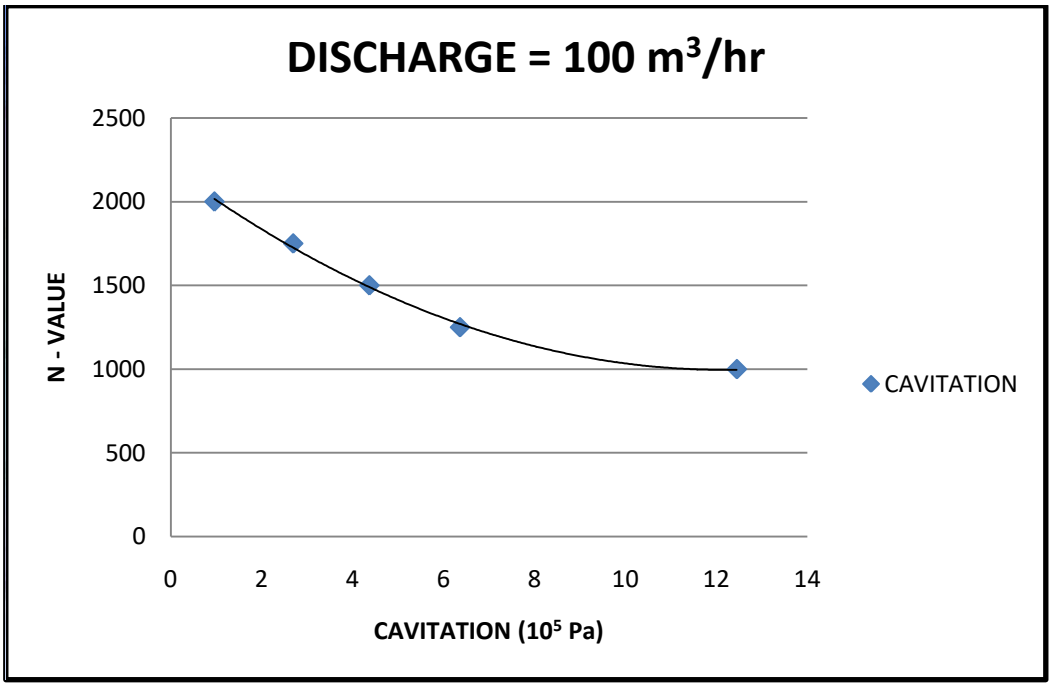

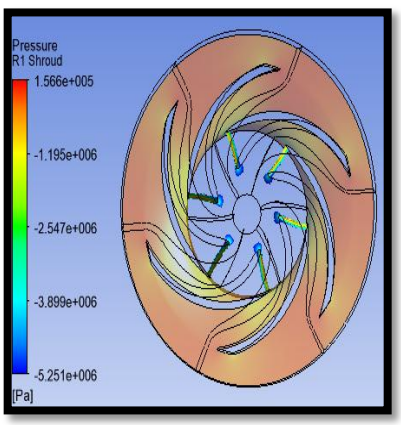

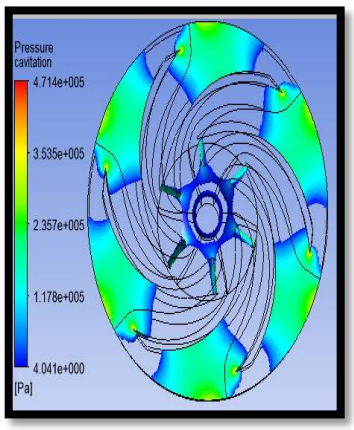

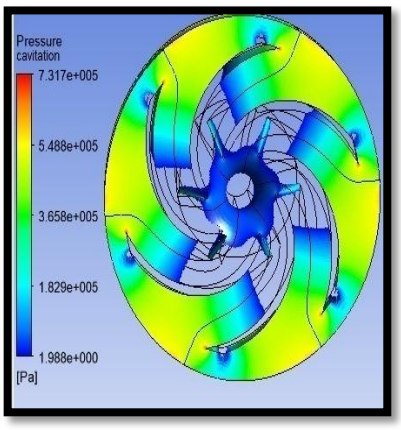

RPM = 2000 **RPM = 1750** **RPM = 1500**

FIGURE 4.14 SHOWS CAVITATION IN CENTRIFUGAL PUMP AT VARIOUS R.P.M. AT CONSTANT DISCHARGE OF 100 m^3/hr

TABLE 4.6 CAVITATION VS R.P.M. AT CONSTANT DISCHARGE = 75 m^3 /hr

R.P.M.	2000	1750	1500	1250	1000
CAVITATION (in 10^5 Pa)	1.024	1.258	1.642	2.342	3.245

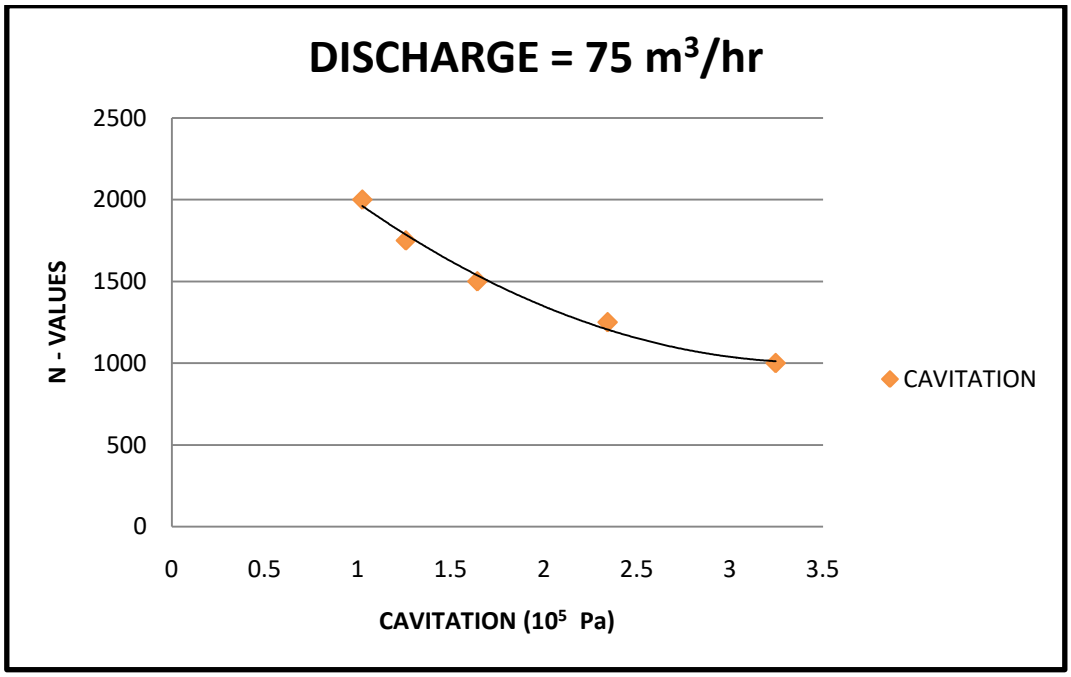

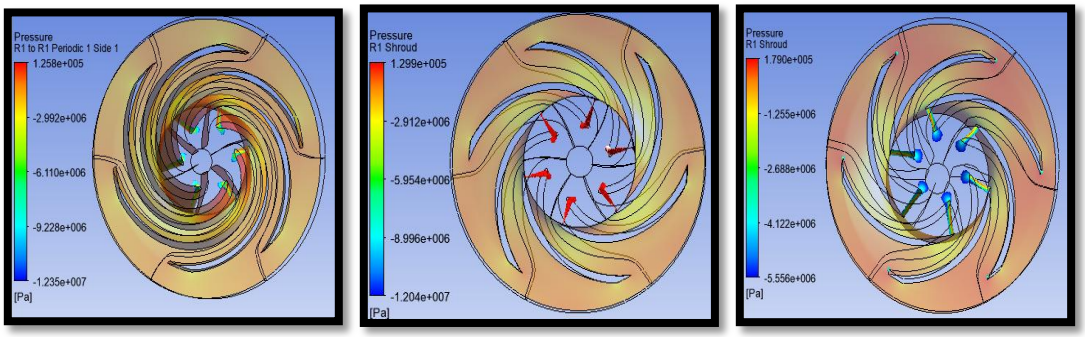

RPM = 2000 **RPM =1750** **RPM = 1500**

FIGURE 4.15 SHOWS CAVITATION IN CENTRIFUGAL PUMP AT VARIOUS R.P.M. AT CONSTANT DISCHARGE OF 75 m^3/h

TABLE 4.7 VARIATION OF BOILING POINT OF WATER WITH ABSOLUTE PRESSURE AND THEIR CORRESPONDING NET POSITIVE SUCTION HEAD AVAILABLE

S. NO.	TEMPERATURE (^{O}C)	$NPSH_A$ (m)	Absolute pressure in KPa
1	0	10.3	0.6
2	5	10.2	0.9
3	10	10.2	1.2
4	15	10.2	1.7
5	20	10.1	2.3
6	25	10	3.2
7	30	9.9	4.3
8	35	9.8	5.6
9	40	9.5	7.7
10	45	9.4	9.6
11	50	9.1	12.5
12	55	8.6	15.7
13	60	8.3	20
14	65	7.8	25
15	70	7.1	32.1
16	75	6.4	38.6
17	80	5.5	47.5
18	85	4.4	57.8
19	90	3.2	70
20	95	1.7	84.5
21	100	0	101.33

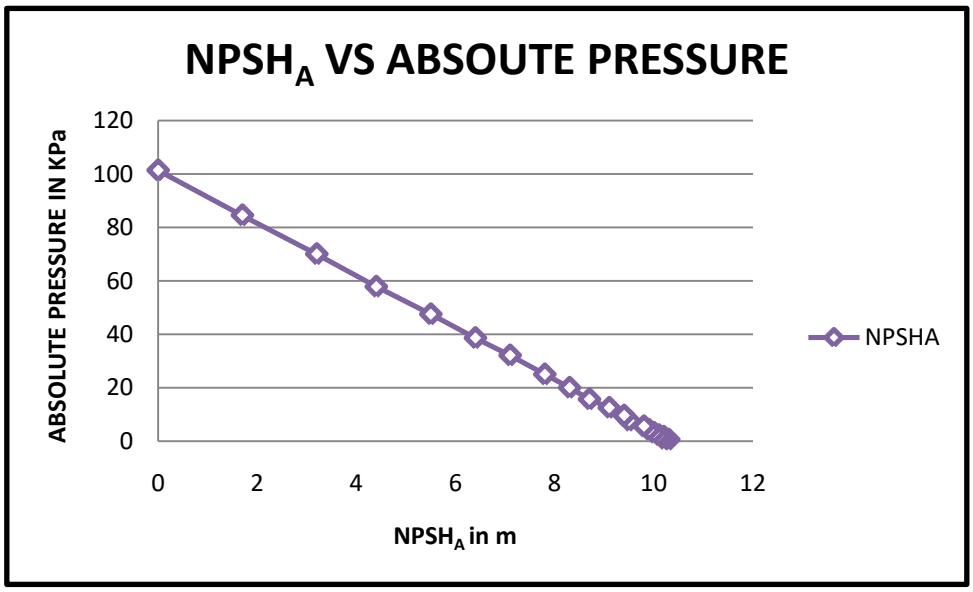

FIGURE 4.16 NPSH$_A$ VS ABSOLUTE PRESSURE CURVE

$$NPSH_A = H_A \pm H_Z - H_F + H_V - H_{VP}$$

H_A = The absolute pressure on the surface of the liquid in the supply tank

H_Z = The vertical distance between the surface of the liquid in the supply tank and the centerline of the pump.

H_F = Friction losses in the suction piping

H_V = Velocity head at the pump suction port

H_{VP} = Absolute vapor pressure of the liquid at the pumping temperature

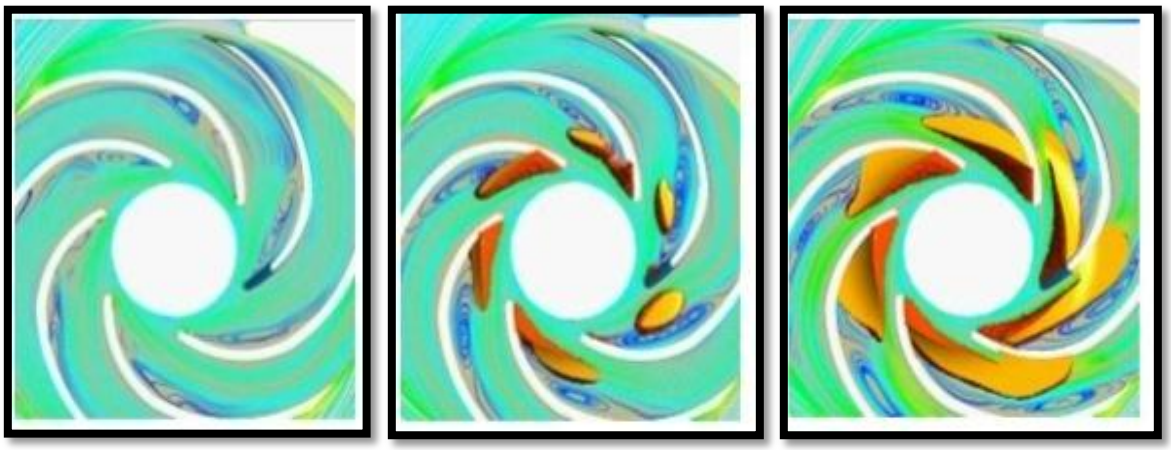

NPSH$_A$ =8.6 m **NPSH$_A$ = 2.91 m** **NPSH$_A$ = 2.03 m**

FIGURE 4.17 NET POSITIVE SUCTION HEAD AT BOILING POINT OF 55^O C

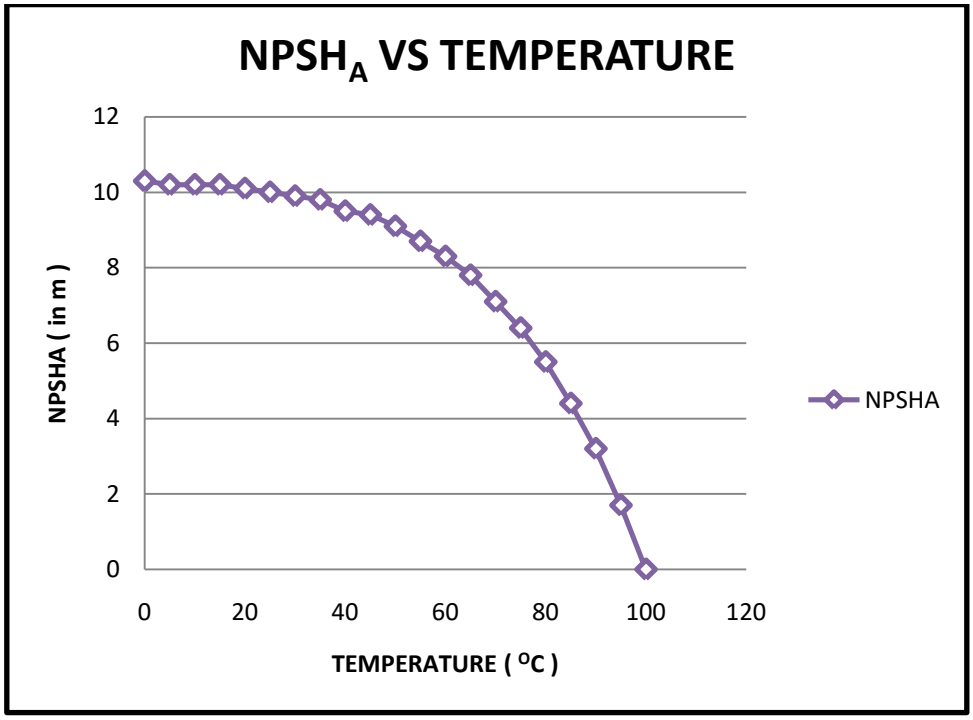

FIGURE 4.18 NPSH$_A$ VS TEMPERATURE CURVE

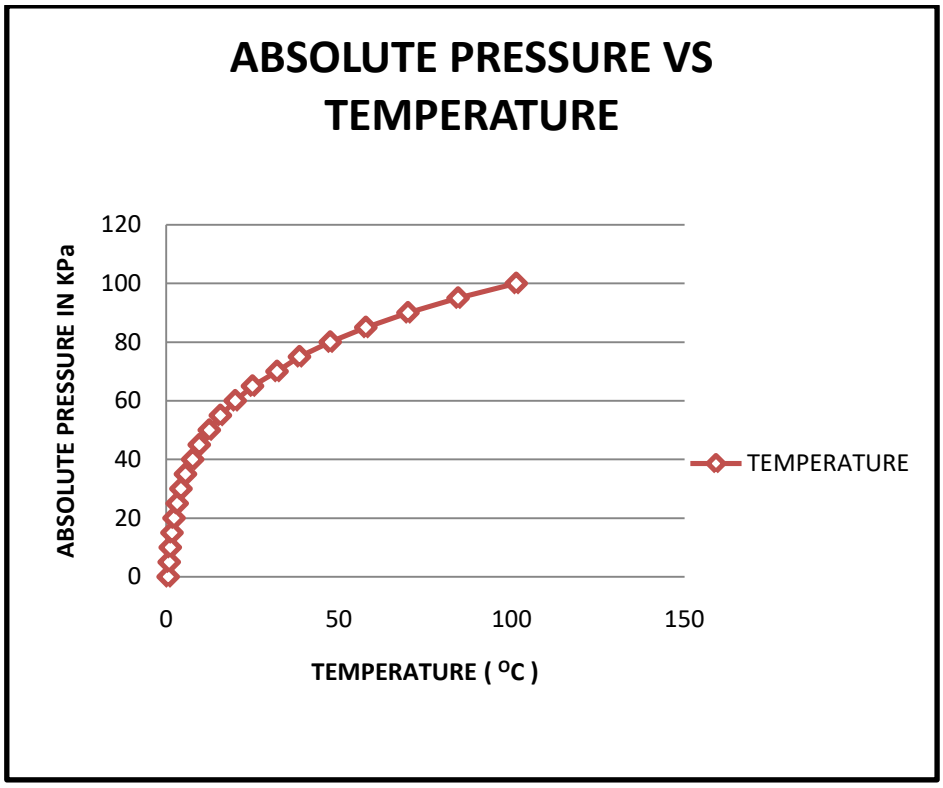

FIGURE 4.19 ABSOLUTE VS TEMPERATURE CURVE

TABLE 4.8 VARIATION OF HEAD, PUMP EFFICIENCY, NET POSITIVE SUCTION HEAD REQUIRED AND POWER WITH CHANGE IN DISCHARGE AT CONSTANT R.P.M 2000

SERIAL NUMBER	DISCHARGE (in m^3/h r)	HEAD (in m)	PUMP EFFICIENCY (in %)	$NPSH_R$ (in m)	POWER (in K-w)
1	20	80.03	30	3.159	11.682
2	40	78.12	50	3.864	16.754
3	60	75.07	66.67	4.667	19.068
4	80	70	72.12	5.000	21.098
5	100	62.89	77.213	6.108	23.766
6	120	52.69	73.136	8.034	25.032
7	140	45.82	67.895	10.231	26.412

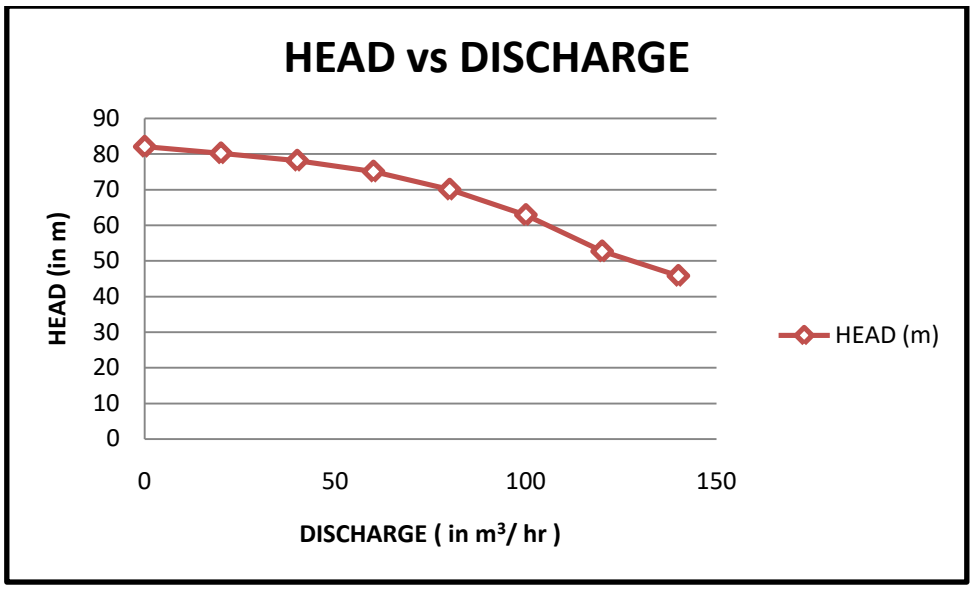

FIGURE 4.20 HEAD VS DISCHARGE CURVE

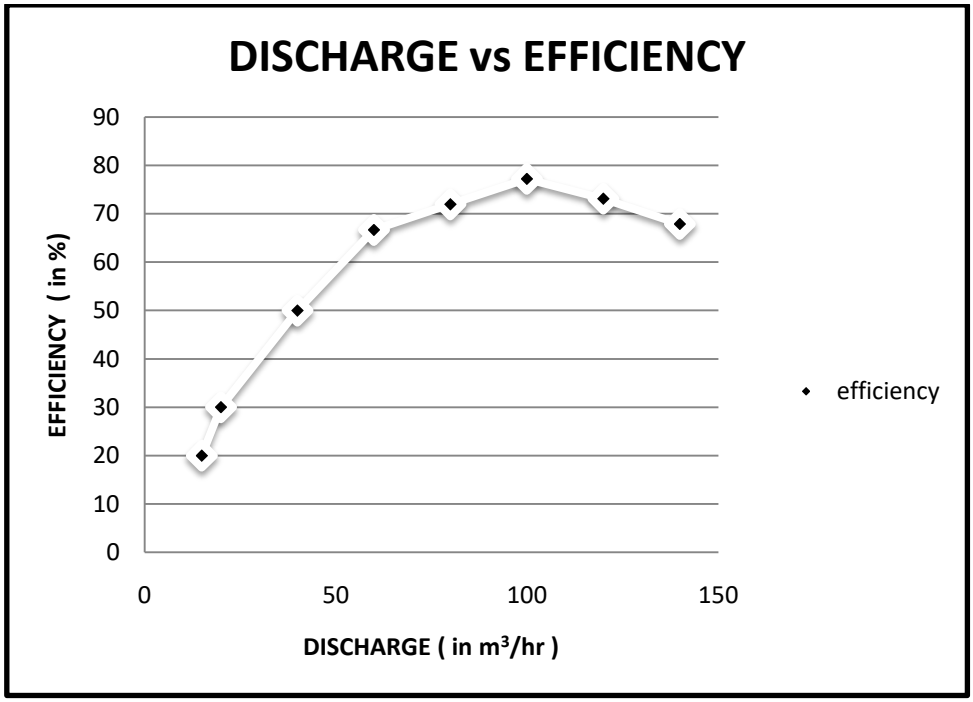

FIGURE 4.21 DISCHARGE VS EFFICIENCY CURVE

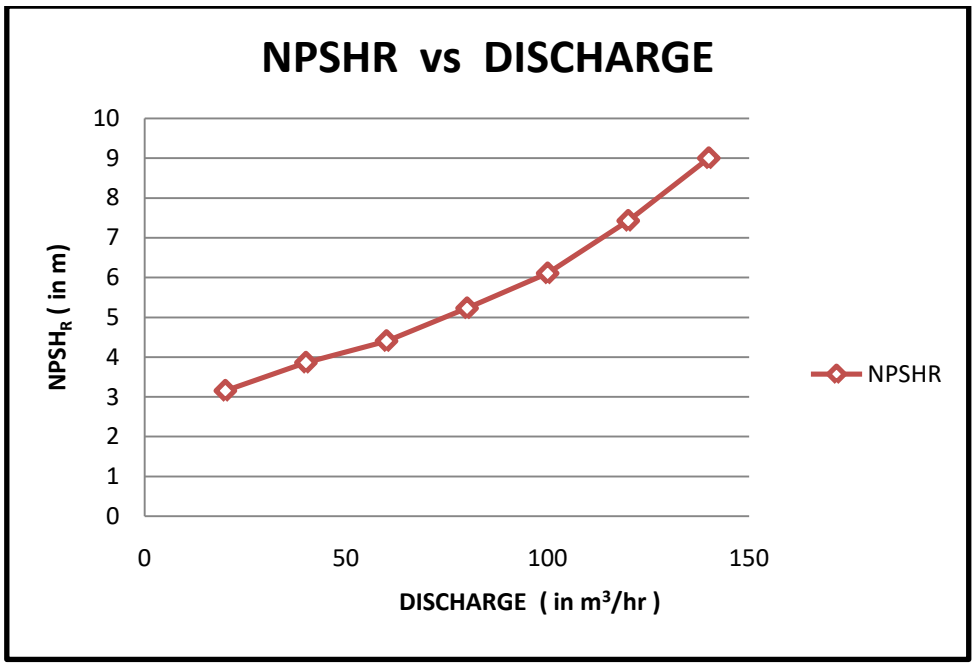

FIGURE 4.22 NPSH$_R$ VS DISCHARGE CURVE

Figure 4.22 shows NPSH$_R$ increases as discharge increases

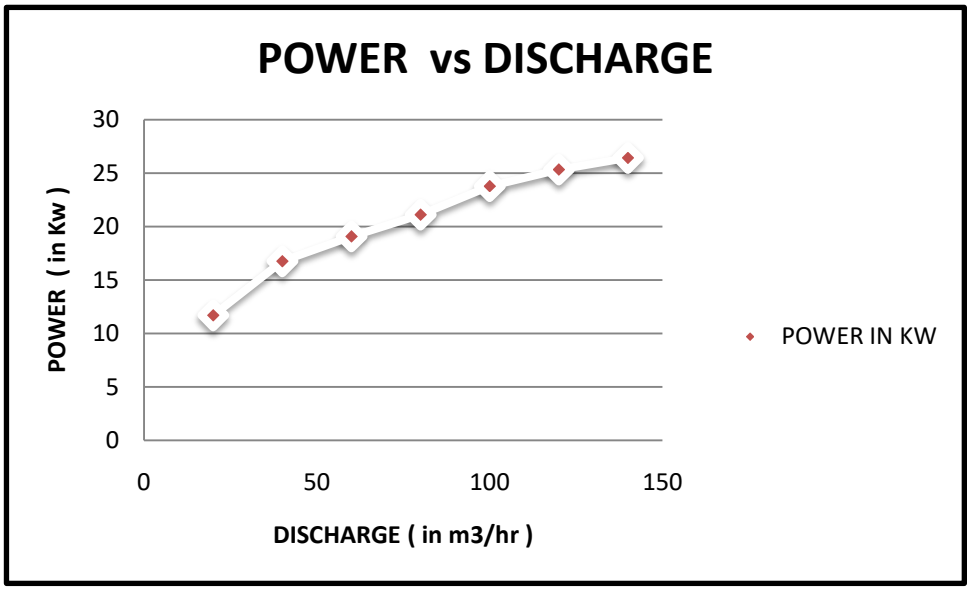

FIGURE 4.23 POWER VS DISCHARGE CURVE

Figure 4.23 shows as discharge increases power obtained increases

OBSERVATIONS

1. As discharge increases cavitation increases because due to increase in discharge at constant area velocity increase and hence velocity head increases, by Bernoulli's theorem summation of pressure head, velocity head and datum head must be constant (considering at ideal condition) hence pressure head decreases and hence cavitation increases.
2. As discharge increases net positive suction head required increases and net positive suction head available decreases hence chance of cavition increases.
3. As discharge increases from 25 m^3/hr to 140 m^3/hr the variation of parameter like power, head, efficiency, and net positive suction head is observed.
4. Maximum cavitation occurring at tip of impeller and at inside surface of blade, to avoid surface pitting at these point we calculate cavitation at this points and take measures to reduce it.
5. To counter the cavitation at higher discharge, increase the R.P.M., as R.P.M. increases cavition reduces.
6. Bubbles create at low temperature and at outlet pressure is high hence these bubbles condenses and burst at surface of pump cause cavitation.
7. As discharge increases efficiency increases up to a particular point, depend on other parameter like r.p.m, blade angle e.t.c. and then start decreasing.
8. Inlet pressure vary boiling point hence at higher pressure cavitation avoided.

CHAPTER 5

CONCLUSIONS

Simulation studies of cavitation in centrifugal pump reveals that –

1. As discharge increases cavitation increases.
2. At constant discharge if rotation speed increases (in RPM), cavitation decreases and vice versa.
3. At minimum discharge and high rotation speed cavitation decreases and vice versa.
4. Increase in temperature of liquid cause increase in cavitation and vice versa.
5. If Net Positive Suction Head Available is kept above some value we can avoid cavitation.
6. As discharge increases head decreases.
7. As discharge increases power generation increases.
8. At high discharge more power we get but efficiency reduces due to cavitation.
9. It is found that we get best efficiency of around 77% at discharge of 100 m^3/hr.
10. By changing parameter like r.p.m., blade angle etc we get higher efficiency at constant discharge.
11. Cavitation also occurs due to air content in water.
12. As air content in water increases more bubble forms and cause cavitation.
13. As air content increases with flow of water, efficiency of system start decreasing and service life of pump reduces.
14. As inlet pressure increases boiling point decreases hence water boils at low temperature.

REFERENCES

(1) Asnaghi, A., Jahanbakhsh, E. & Seif, M. S., 2010. Unsteady Multiphase Modelling of Cavitation Around NACA 0015. Journal of Marine Science and Technology , 18(5), pp. 689-696.

(2) Bacharoudis, E. C., Filios, A. E., Mentzos, M. D. & Margaris, D. P., 2008. Parametric Study of a Centrifugal Pump Impeller by Varying the Outlet Blade Angle. The Open Mechanical Engineering Journal, Volume 2, pp. 75-83.

(3) Balasubramanian, R., Sabini, E. & Bradshaw, S., 2011. Influence of Impeller Leading Edge Profiles on Cavitation and Suction Performance. Proceedings of the Twenty-Seventh International Pump Users Symposium.

(4) Barrio, R., Fernandez, J., Parrondo, J. & Blanco, E., 2010. Performance Prediction of a Centrifugal Pump Working in Direct and Reverse Mode Using Computational Fluid Dynamics. International Conference on Renewable Energies and Power Quality, March.

(5) Brennen, C. E., 1995. Cavitation and Bubble Dynamics. New York: Oxford University Press.

(6) CD-Adapco, 2013. User Guide Star CCM+ Version 8.06.

(7) Davidson, L., 2011. An Introduction to Turbulence Models, Chalmers University of Technology, Goteborg, Sweden.)

(8) De Beristain, I. G., 2012. Aerodynamic Analysis of Fan Unsteady Simulations, MSc Dissertation, University of the Basque Country, Leioa, Spain.

(9) De Souza, A., 2013. NAFEMS-CFD Jargon Explained. [Online] Available at: http://www.nafems.org/join/resources/cfdjargon/

[Accessed March 2013].

(10) Hellstroom, F., Gutmark, E. & Fuchs, L., 2012. Large Eddy Simulation of the Unsteady Flow in a Radial Compressor Operating Near Surge. Journal of Turbomachinery, Volume 134.

(11) Jafarzadeh, B., Hajari, A., Alishahi, M. M. & Akbari, M. H., 2010. The Flow Simulation of a LowSpecific-Speed High-Speed Centrifugal Pump. Applied Mathematical Modelling, Volume 35, pp. 242-249.

(12) Liuzzi, D., 2012. Two-Phase cavitation Modelling, Ph.D Dissertation, University of Rome, Rome, Italy.

(13) Lucius, A. & Brenner, G., 2010. Unsteady CFD Simulations of a Pump in Part Load Conditions Using Scale-Adaptive Simulation. International Journal of Heat and Fluid Flow, Volume 31, pp. 11131118. Martensson, H., Andersson, S., Trollheden, S. & Brodin, S., 2008. Rocket Engines: Turbomachinery. NATO R&T.

(14) Montomoli, F., Massini, M. & Salvadori, S., 2010. Geometrical Uncertainty in Turbomachinery: Tip Gap and Fillet Radius. Computers and Fluids, Volume 46, pp. 362-368.

(15) Pope, S. B., 2000. Turbulent Flows. Cambridge: Cambridge City Press.

(16) Qiu, X., Anderson, M. & Japikse, D., 2010. An Integrated Design System for Turbomachinery. Journal of Hydrodynamics, 22(5), pp. 358-365.

(17) Ranade, V. V. & Krishnan, Y., 2002. CFD Predictions of Flow Near Impeller Blades in Baffled Stirred Vessels: Assessment of Computational Snapshot Approach. Chemical Engineering Communications, Volume 189, pp. 895-922.